University of Pisa
School of Engineering

“Characterization of a new digital acquisition system for microdosimetry using a tissue equivalent proportional counter (TEPC)”

Supervisors: Dr. Eng. Riccardo Ciolini (University of Pisa)
Dr. Sabina Chiriotti Alvarez (SCK-CEN)

Candidate: Gerardo Chiavacci

ACADEMIC YEAR 2015-1016

Table of contents

Introduction

Microdosimetry studies the probability distribution of the imparted energy when an ionizing particle crosses site size in order of the *μm.*

The Tissue Equivalent Proportional Counter (TEPC) is a microdosimetric instrument that measures radiation dose and dose equivalent in complex radiation fields (fields containing a mixture of particle types).

The signal processing chain convert the signal from the TEPC in a pulse signal and measure the pulse height distributions which correspond to an energy deposition distribution in the simulated microscopic volume of the detector.

The aims of this work are:

- To perform a systematic investigation with a new digital acquisition system: by testing the resolution, input counting rate, dynamic range, stability and reproducibility.
- To optimize the electronic chain.
- To perform microdosimetric measurements with a TEPC with gamma and neutron sources.

Lineal energy distributions for neutrons and gamma rays were measured using a TEPC with three different preamplifiers and with both acquisition systems, Inspector from Canberra and the DT5780 from CAEN. A series of measurements were performed with the counter filled with propane-based tissue equivalent gas at operating gas pressure corresponding to a site size of 2.0 *μm* in diameter.

Chap. 1. Microdosimetry

In its action on matter, ionizing radiation is uniquely efficient because it transfers energy to atoms in a highly concentrated form. This absorbed energy is transformed into initial molecular changes or degraded into heat in a period that is generally less than 1 microsecond. In this brief time interval many highly complex interactions occur before reasonably stable molecular species are produced.

The average energy absorbed per unit mass of irradiated medium, the absorbed dose, is minute compared to the energy deposited densities. The effectiveness of ionizations is further enhanced by their association in the tracks of charged particles. Thus while the absorbed dose is a useful and standard quantity in the specification of irradiation, effects depend on the pattern in which a given amount of energy is deposited in the irradiated medium. A knowledge of such energy distributions is required not only in any explanations of the relative effectiveness of different kinds of ionizing radiation but it also can be expected to provide insight into the action of ionizing radiation in general. [3]

Microdosimetry is a technique for measuring the microscopic distribution of absorbed energy due to ionizing radiations. Like other branches of physics microdosimetry has experimental and theoretical aspects. The former deals with the measurement of microdosimetric quantities and the latter is concerned with relations between these, and other more general, physical quantities. The experimental approach is based on the concept of sites that are regions of specified dimensions in which the energy absorbed from ionizing radiations is considered without regard to its microscopic distribution within a site**.** The energy imparted is measured event by event inside a tissue equivalent simulated site with a diameter of the order of micrometers. [3]

In figure 1.1 the specific energy deposited by an ionizing particle versus the volume that the particle is crossing is shown. Here it’s clear the difference between the conventional dosimetry (that refers to the absorbed dose, which is a quantity defined by the energy deposited in macroscopic volumes) and the microdosimetry (that refers to the statistical variations of imparted energy by an ionizing particle in microscopic volume).

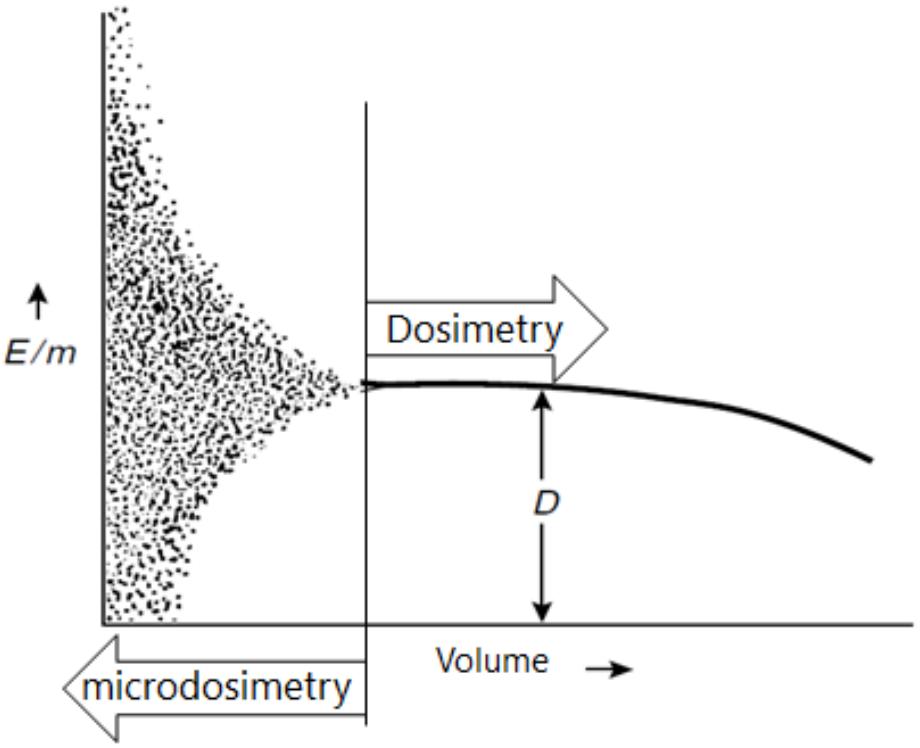

Figure 1.1 - Graphic explanation of the differences between dosimetry and microdosimetry. Specific energy deposited by an ionizing particles E/m versus the volume that the particles is crossing.

By interpretation of the event-size spectrum recorded during the measurement, valuable information can be obtained enabling some analysis of the radiation field to be made. Applications of microdosimetric techniques allow the use of lineal energy (energy imparted by a single event divided by the mean chord length of the cavity, better defined in cap. 1.1) event-size spectra (microdosimetric spectra) to determine the values of the dose contribution by different types of particles, to understand the mechanisms of radiation interaction physics, and enabling the measurement of absorbed dose, dose equivalent and mean quality factor as well as a physical means of quantifying radiation quality with regards to biological effects. The fundamental quantity applied in microdosimetry studies is the energy deposited in *Joule* (or *eV*). The imparted energy is the energy deposited in a single interaction, and it is the energy that a charged particle loses when it passes through a tissue equivalent proportional counter (TEPC) gas cavity. This can be related to the energy which would be lost along a microscopic path length. A single interaction event in the cavity gas will produce a charge that is converted to a voltage pulse which amplitude is proportional to the amount of imparted energy. The frequency of events measured for different event-sizes allows the absorbed dose to be determined. The dose equivalent can be evaluated by the same method using an appropriate quality factor approximation. [6]

1.1. Definition of microdosimetric quantities

The fundamental quantity applied in microdosimetry is the energy deposited in a single event 'ε'. To be used more easily the energy deposited in a single interaction need to be converted in lineal energy '*y*' using a geometric factor. The lineal energy is defined as the energy deposition by a single event divided by the mean chord length of the cavity '$\bar{l}$'.

$$y = \frac{\varepsilon}{\bar{l}}$$

Lineal energy is presented in units of keV/μm.

The lineal energy *y* is the stochastic analog to the lineal energy transfer (LET) quantity with the difference that LET is not measurable in mixed radiation fields and it gives no information on the energy distribution. Another equally important quantity to be defined in microdosimetry is the specific energy *z*, defined as the ratio of the imparted energy to a given volume of mass *m*. The unit of specific energy *z* is joule per kilogram (J/kg), which is usually expressed as Gray (Gy). For a single event, the relation between lineal energy *y* and specific energy *z* differs by a numerical factor that depends on the geometry of the site and density of the gas.

When particles interact with a given volume, they can release, with different probabilities different quantities of energy, which generate a broad spectrum of lineal energy. The distribution of the number of events with event size between *y* and *y+dy* shall be denoted the frequency distribution as *f(y)* of *y.*

The dose distribution *d(y)* is defined as the normalized distribution of the product *yf(y)* and represent the relative contribution of the event *y* to the dose.[11][16]

1.2. Representation of microdosimetric distributions

Since the range of event sizes, and so pulse heights, would cover several orders of magnitude (from fractions of eV to hundreds of keV) the way to represent the microdosimetric distributions need to be analyzed. In the present work the problem of dealing with a large range of pulse sizes is being managed by redistributing the measured data, in order to better present the obtained information from the data and to aid its interpretation. The raw information is modified by redistributing the data onto a scale formed of *N* (normally between 40 and 60) equal logarithmic intervals (or bins per decade, for 5 decades) of lineal energy. This procedure is called *rebinning*. [5][6]

The rebinning, or redistribution of the event-size data, is achieved step by step.

To create the logarithmic intervals the formula $y(i) = y(0)*10^{(i/N)} = 10^{X/N}$ was used, where *X* represents an index of the logarithmic bin number. For example, if we want to use *N* = 40 and 5 decades (from 0.01 keV/μm to 1000 keV/μm) we will have as

first value *X* = -80 (which represents a linear energy value of *y* = 0.01 keV/μm) and as last value *X* = 120 (which represents a linear energy value of *y* = 1000 keV/μm).

In figure 1.2 a representation of the equal logarithmic intervals creation procedure is shown.

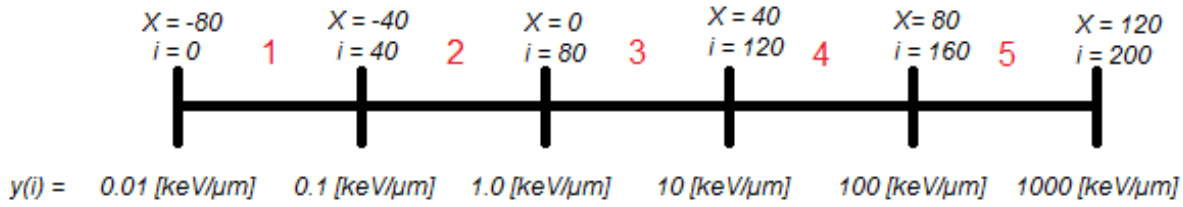

Figure 1.2 – Equal logarithmic intervals creation procedure (5 decades).

The basic mathematical idea behind the creation of new bins width is that the ratio between the differential of the logarithmic value (*dLn(y)*) and the linear value (*dy*) for an event-size interval is equal to 1/*y*.

The width of the i-th logarithmic interval (so the change in the lineal energy from a bin center, $y_{i-1/2}$, to another one, $y_{i+1/2}$) is given by:

$$\Delta y(i) = y(i) \cdot \left(10^{\frac{1}{2N}} - 10^{-\frac{1}{2N}}\right) = 10^{\frac{X}{N}} \cdot \left(10^{\frac{1}{2N}} - 10^{-\frac{1}{2N}}\right)$$

In figure 1.3 a representation of $\Delta y(i)$ is shown.

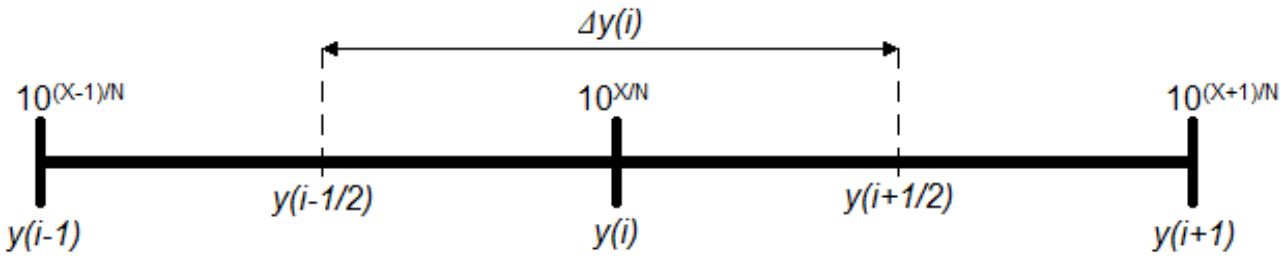

Figure 1.3 – Representation of the i-esim logarithmic interval.

Where i = {0,...,D*N} and D = number of decades, in our case we have a number of bins that is equal to i_{max} = 200 (so the logarithmic scale is subdivided into 200 *y*-values) and:

$$\Delta y(i) = 10^{\frac{X}{40}} \cdot \left(10^{\frac{1}{80}} - 10^{-\frac{1}{80}}\right)$$

The constant value 0.0576 represents a measure of the distance between two energy points centered in the *y(i)* lineal energy point. So in our case the value of the width of the i-th logarithmic interval $\Delta y(i)$ is given by:

$$\Delta y(i) = y(i) \cdot 0.0576.$$

The number of counts *N(y(i))* falling in each logarithmic interval of width $\Delta y(i)$ are averaged, obtaining the rebinned counts. The spectrum is then represented in count density:

$$n\big(y(i)\big) = \frac{N(y(i))}{\Delta y(i)}$$

The next step is the conversion of the pulse height spectrum *n(y)* in the frequency distribution *f(y)* and dose density distribution *d(y)* of the lineal energy *y*.

Frequency *f(y(i))* and dose density distributions *d(y(i))* are calculated as:

$$f(y(i)) = \frac{n(y(i))}{\sum_{y0}^{ymax} n(y(i)) \cdot \Delta y(i)}$$

$$d(y(i)) = \frac{y(i) \cdot f(y(i))}{\sum_{y0}^{ymax} y(i) f(y(i)) \cdot \Delta y(i)}$$

Here *f*(y) refers to the number of events occurring between event sizes *y* and *y+dy.* Mathematically speaking, since the frequency distribution is in fact a probability density of *y* it can be normalized to unity in terms of a linear scale. Since in our work we used a logarithmic scale of *y* instead to integrate on the linear interval *dy* we replaced it with the logarithmic interval *dLn(y)*.

$$\int_0^\infty f(y)dy = 1 \rightarrow \int f(y) \cdot [y \cdot dLn(y)] = Ln(10) \int y \cdot f(y) \cdot dLog(y) = 1$$

The frequency at which events of a given size occur is not that much of interest as the fraction of the total absorbed radiation energy which is deposited by the events of a given size. From the frequency distribution we calculated the dose distribution, representing the fraction of the absorbed dose deposited by events within a specified event-size range: *yf(y)* represents the dose distribution *d(y)*, which is the total amount of kinetic energy deposited in the gas cavity by the associated charged particles. The logarithmic representation of the normalized dose distributions is expressed as:

$$\int_0^\infty d(y)dy = 1 \rightarrow \int d(y) \cdot [y \cdot dLn(y)] = Ln(10) \int y \cdot d(y) \cdot dLog(y) = 1$$

The representation of the microdosimetric spectra is then in a semi-logarithmic scale,

yd(y) (in the vertical axis) vs. *Log(y)* (in the horizontal axis).

The last quantities that need to be defined are the frequency-mean lineal energy $\overline{y_F}$ and the dose-mean lineal energy $\overline{y_D}$:

$$\overline{y_F} = \sum_{y_0}^{y_{max}} y_i \cdot f(y_i) \cdot \Delta y_i$$

$$\overline{y_D} = \sum_{y_0}^{y_{max}} y_i \cdot d(y_i) \cdot \Delta y_i$$

In figure 1.4 an example of how the data presentation can be improved is shown.

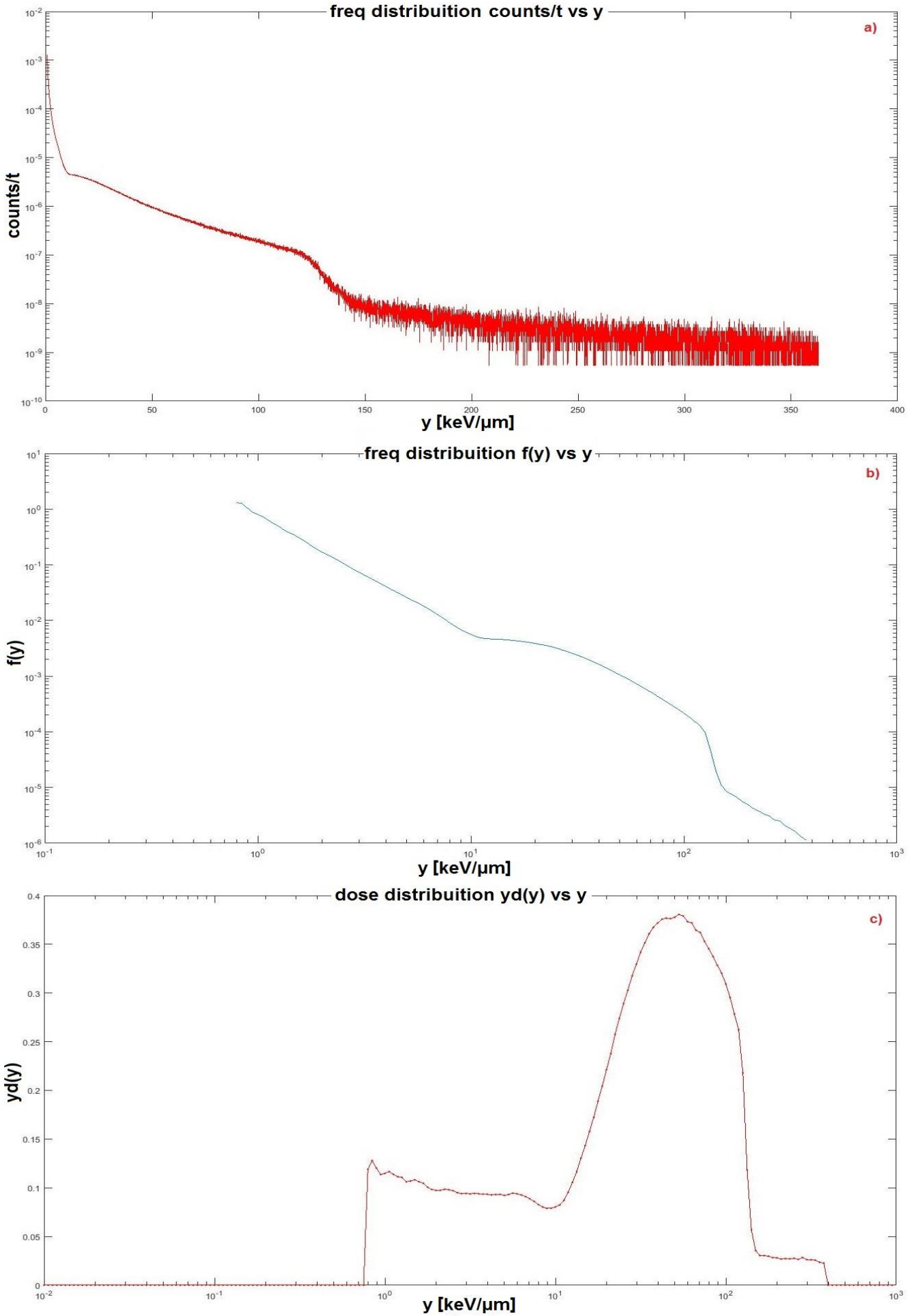

Figure 1.4 – Example of improvement in data presentation achieved by rebinning.

Chap. 2. TEPC

To detect the presence of ionizing particles it is possible to use a wide range of radiation detection instruments. In particular, gaseous ionization detectors use the ionizing effect of radiation upon a sensor. All of these have the same basic design of two electrodes separated by air or a special fill gas. If a particle has enough energy to ionize a gas atom or molecule, the resulting electrons and ions cause a current flow which can be measured. The radiation entering the counter volume (normally spherical or cylindrical) collides with an atom of the inert gas and ionizes it producing an electron and a positively charged ion, called "ion pair". As the charged particle travels through the chamber it leaves a trail of ion pairs along its trajectory, the number of which is depending from the applied voltage.

The three basic types of gaseous ionization detectors are ionization chambers, proportional counters, and Geiger-Müller tubes. The strength of the electric field between the electrodes and the type and pressure of the fill gas determines the detector's response to ionizing radiation.

Ionization chambers operate at low electric field strength, selected such that no gas multiplication takes place. Ion chambers are preferred to the other two types for high radiation dose rates because they have no "dead time". The dead time is the time after each event during which the system is not able to record another event. This phenomenon affects the accuracy of proportional counter and Geiger Muller tube at high dose rates.

Geiger-Müller tubes operate at high electric field strength, where the proportionality between the radiation energy deposited and the amplitude of the output signal is lost. Because the output pulse from a Geiger-Müller tube is always the same magnitude regardless of the energy of the incident radiation, the tube cannot differentiate between radiation types. For this reason they can be used just as counter.[10] The main application of Geiger-Müller tube is in Geiger counters that is a robust and inexpensive detector.

A proportional counter uses a combination of the mechanisms of a Geiger–Müller tube and an ionization chamber, and operates in an intermediate voltage region between these. The key feature of proportional counters is the ability to measure the energy of incident radiation, by producing a detector output that is proportional to the radiation energy. The design goal is that each original ionizing event due to incident radiation produces only one avalanche. This is to ensure proportionality between the number of original events and the total ion current. For this reason the applied

voltage, the geometry of the chamber and the diameter of the anode wire are critical to ensure proportional operation. The chamber geometry and the applied voltage are such that in most of the chamber the electric field strength is low and the volume acts as an ion chamber.

However, the field is strong enough to prevent re-combination of the ion pairs and causes positive ions to drift towards the cathode and electrons towards the anode. This is the "ion drift" region. In the immediate vicinity of the anode wire, the field strength becomes large enough to produce electrons avalanches. This avalanche region occurs fractions of a millimeter from the anode wire. The purpose of this avalanche is to have an amplified output signal that can actually be measured. The process of charge amplification greatly improves the signal-to-noise ratio of the detector and reduces the subsequent electronic amplification required. [10]

The Tissue Equivalent Proportional Counter (TEPC) is a gas proportional counter widely used to characterize the radiation field in radiation therapy and radiation protection. In a tissue equivalent proportional counter the fill gas of the chamber is a tissue-equivalent gas and the wall of the chamber is made of a tissue equivalent plastic.

So in the case of a TEPC the energy that a charged particle loses when it passes through the gas cavity can be related to the energy which would be lost along a microscopic path length within a tissue medium of unit density. The distribution of the deposited energy will be related to LET (Linear Energy Transfer) of the radiation. The density difference between the gas and the tissue enables the simulation by the counter of a microscopic tissue volume. A single interaction event in the cavity gas will produce a voltage pulse of measured amplitude proportional to the amount of imparted energy. The frequency of events measured for different event-sizes allows the absorbed dose to be determined.[23]

2.1. Physical characteristics of our TEPC

The detector used in this work is a spherical tissue equivalent proportional counter. It is filled with a tissue equivalent gas at reduced pressure (880 Pa for a 2µm simulated diameter with propane-based TE gas). An aluminum shell is used as a vacuum tight container for the sphere and is mounted on an aluminum plate, which holds the electrical and gas connection. The instrument is used to accumulate a pulse height spectrum proportional to the energy deposited in the sensitive volume. In figure 1.5 the scheme of the TEPC is shown, with the following components.

A. Sphere, 4.94" id, 0.084 wall thickness, A-150 Tissue Equivalent Plastic.

B. Central Electrode, 0.003" diameter SS wire.

C. ^{244}Cm Source Rod, 0.062" diameter x 0.115 long, (points up when off).

D. Cover, 0.050" thick Aluminum, 6.00"id.

E. Baseplate, 0.50" thick Aluminum.

F. Brass bellows valve.

G. Brass quick-connect.

The end plate carries the signal and high voltage connectors. The center wire of the high voltage cable should be positive with respect to the shield, so that we can collect the electrons (that are faster than the positive ions) on the central wire. [23]

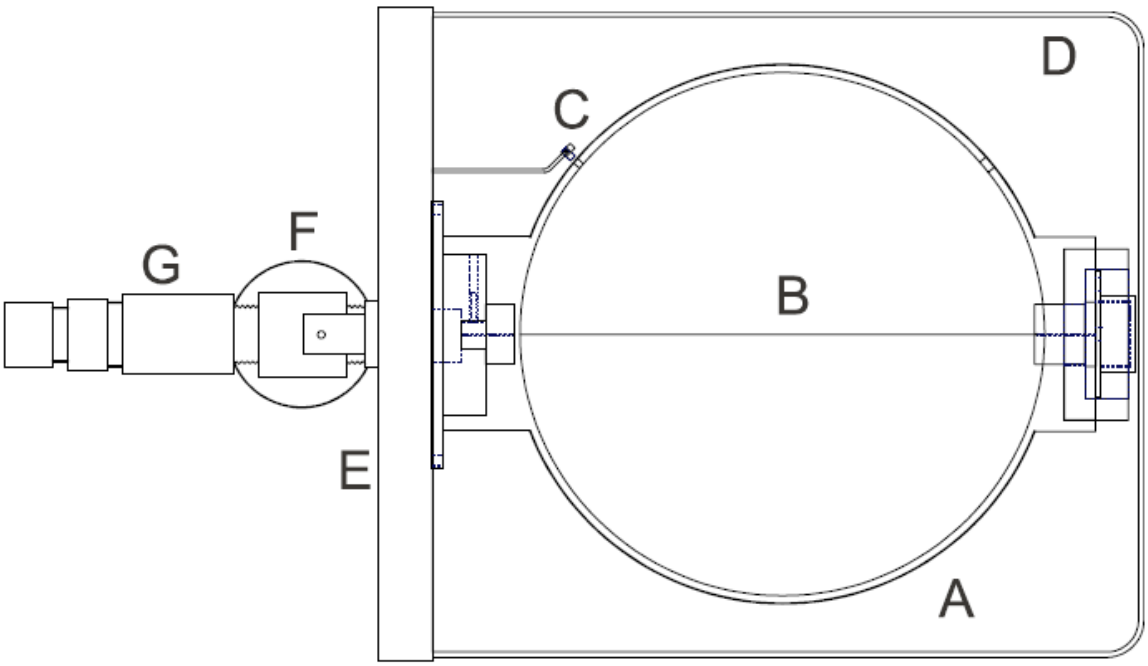

Figure 1.5 - Scheme of the TEPC.

2.2. TEPC calibration

The TEPC is calibrated in terms of lineal energy, by exposing it to an internal alpha source (^{244}Cm). The source is positioned so that the ^{244}Cm alpha particles can enter the sphere through a collimator when the connector plate is horizontal and the writing on the base is upside down. Referring to the Figure 1.5, the source is turned ‘on’ when the TEPC is put in such a way that the connector plate is on the upper position. The source is "off" when the connector plate is horizontal and the writing on the base is facing up. ^{244}Cm has a mean alpha energy of 5.80 MeV which, on averages, corresponds to 81.72 *keV/μm* over a range of 1*μm* in tissue. For a spherical counter of diameter 'd', the mean chord length is *l* = (2/3)d. Because of the collimator, the source produces a peak on a multichannel pulse height analyzer. The center of this distribution is characteristic of the stopping power of the alpha particles (i.e., of the LET of the alpha particle in tissue equivalent material) and the site size, so we can calculate the energy loss from the particles that completely passes through the site. Then, from the definition of lineal energy '*y'* we can calculate the calibration factor for the conversion between channels and lineal energy. Gaussian fitting of the spectra is performed in order to find the precise position of the maximum. The resulting alpha source resolution is relatively poor due to a compromise between source strength, collimator opening and useful count rate. [1]

It is also possible to perform the calibration of TEPCs without an internal alpha source. This alternative method is based on the upper edges of the microdosimetric spectrum, which correspond to the maximum energy imparted by particles in the cavity (so that we can have proton edge or electron edge). For this energetic calibration way we need to know the radiation field that we are measuring. TEPC collects data as a function of time to measure the dose rate and estimate the dose equivalent by making spectral measurements of the lineal energy loss of the radiation as it passes through the detector volume. The omni-directional detector is surrounded by a tissue equivalent plastic and the internal gas (propane mixture) provides an energy deposition response similar to human tissue: the detector gas is at a very low pressure such that the mass of the gas is approximately that of a cell. TEPC is an automatic microdosimetry system. The detector unit is attached directly to the multi-channel analyzer (MCA) [2] and the output file from the acquisition system software is counts vs. channels file. Once that the calibration factor is calculated, it is possible to have the data in the form of counts vs lineal energy. From this, it is possible to calculate the dosimetric and microdosimetric quantities, as explained in chapter 1.

2.3. Tissue equivalent gas and refilling procedure

Gas purity is of considerable importance in counter operation. Propane based tissue equivalent (TE) gas was chosen to fill the TEPC in this work. The gas has the following composition: 55% C_3H_8, 39.6% CO_2 and 5.4% N_2. Poor resolution, gain or low voltage arc-over point are evidences of gas problems. [7]

The usual procedure to fill the detector is described in the TEPC manual.[23] It starts with a pump to have a vacuum down to 1.33 Pa. The counter is then filled to about 66.6612 kPa with tissue equivalent gas and pumped down to 1.33 Pa. This procedure may be repeated if the counter has not been in use for some time. Pump down and filling should be slow to avoid contaminating the detector with the optional alpha source. Alpha particles may be forced into the detector from the gas flowing by the source. The indication is to fill the detector with it in the horizontal position and the writing on the base right side up because this positions the source is away from the gas flow. The counter is next filled to the proper pressure for operation.

The spherical cavity of the TEPC was filled with the TE gas to a low pressure determined by the TE gas density in order to simulate a specified microscopic site in tissue. In our study we simulated a 2 μm microscopic size diameter. In the following table the trend of TE gas pressure in function of the ambient temperature is shown.

To do the refilling a vacuum pump and gas handling system was used. In figure 1.6 the used system is shown. In figure 1.7 the TE gas bottle is shown.

Table 1.1 - Trend of TE gas pressure in function of the ambient temperature.

Temperature (°C)	Temperature (K)	Pressure (Pa)	Pressure (atm)
18.0	291.15	873.99	0.0086525
18.2	291.35	874.59	0.0086585
18.4	291.55	875.19	0.0086644
18.6	291.75	875.79	0.0086703
18.8	291.95	876.39	0.0086763
19.0	292.15	876.99	0.0086822
19.2	292.35	877.59	0.0086882
19.4	292.55	878.19	0.0086941
19.6	292.75	878.79	0.0087001
19.8	292.95	879.39	0.0087060
20.0	293.15	880.00	0.0087120
20.2	293.35	880.60	0.0087179
20.4	293.55	881.20	0.0087238
20.6	293.75	881.80	0.0087298
20.8	293.95	882.40	0.0087357
21.0	294.15	883.00	0.0087417
21.2	294.35	883.60	0.0087476
21.4	294.55	884.20	0.0087536
21.6	294.75	884.80	0.0087595
21.8	294.95	885.40	0.0087654

Figure 1.6 – The vacuum and gas handling system.

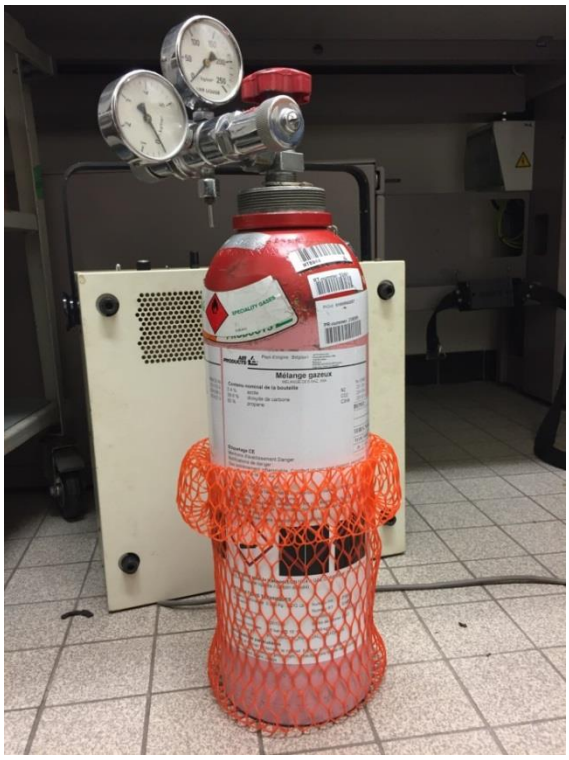

Figure 1.7 – Tissue equivalent gas bottle.

Signal processing

Chap. 3. The Charge Sensitive Preamplifier

In a TEPC radiation interactions with the gas atoms result in the creation of a number of ion pairs (electrons and partially ionised gas atoms) proportional to the energy deposited by the incident radiation. This generated ion pairs are accelerated by an electric field generated from a difference of potential between two zones of the detector. So the electric field causes the electrons to drift towards the anode where the field strength is highest. The energy of the electrons increases and collisions with other gas atoms cause further ionisation producing more electrons. These secondary electrons themselves drift and acquire enough energy to cause further ionisation (and electrons), and so a large cloud of electrons arrives at the anode in a process known as an avalanche. The quantity of charge produced in the avalanche is still proportional to the energy deposited by the ionising radiation. So the result at the output of the TEPC is a negative current pulse in which the area is proportional to the energy deposited by the radiation: this negative pulse is great enough to be detectable in a Charge Sensitive Amplifier connected to the anode. TEPC are operated in pulse mode to record each individual event that interacts with the sensitive volume.[9]

In the detector used in this work the thin metal wire (anode) is held at a positive potential with respect to the sphere (actually a negative voltage is applied to the sphere). The electrons from the avalanche are collected on the anode that guides them towards the readout electronics. The output signal from the TEPC is a negative pulse which goes to a Charge Sensitive Preamplifier, the first step of the signal processing chain. The output of the Charge Sensitive Preamplifier is a voltage pulse that needs to be analysed. For this reason it is converted into digital numeric values that can be manipulated by a computer. The data acquisition is defined as the process of sampling signals that measure real world physical condition and converting the resulting samples into digital numeric values. In figure 2.1 the electronic chain needed for the acquisition of the signal from the TEPC is shown.

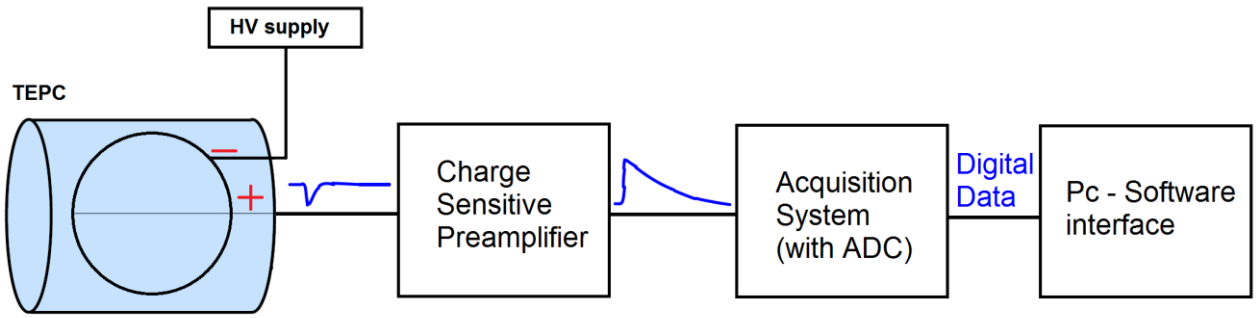

Figure 2.1 – The electronic chain for the signal acquisition. ADC means Analogic to Digital Converter.

A charge sensitive preamplifier is a charge integrator that produces a voltage output proportional to the integrated value of the input current. This is effectively a measurement of the electrical input charge, hence the circuit acts as a charge-to-voltage converter. The integrating capacitor is put in parallel with a discharging resistor, so that the preamplifier output will have pulses with a fast rise time and a long exponential tail with decay time τ.

The charge-amplitude proportionality is set by the capacitor value $V_{out} = \frac{Q}{C}$, where Q is the area of the negative current pulse at the output of the TEPC, and the decay time of the output signal is $\tau = RC$. The charge information (proportional to the energy released by the particle in the detector) is therefore represented by the pulse height: the gain of the circuit depends on the values of the feedback capacitor and the feed-in resistor.[17] In figure 2.2 the signal processing from the TEPC to the output of the Preamp is shown.

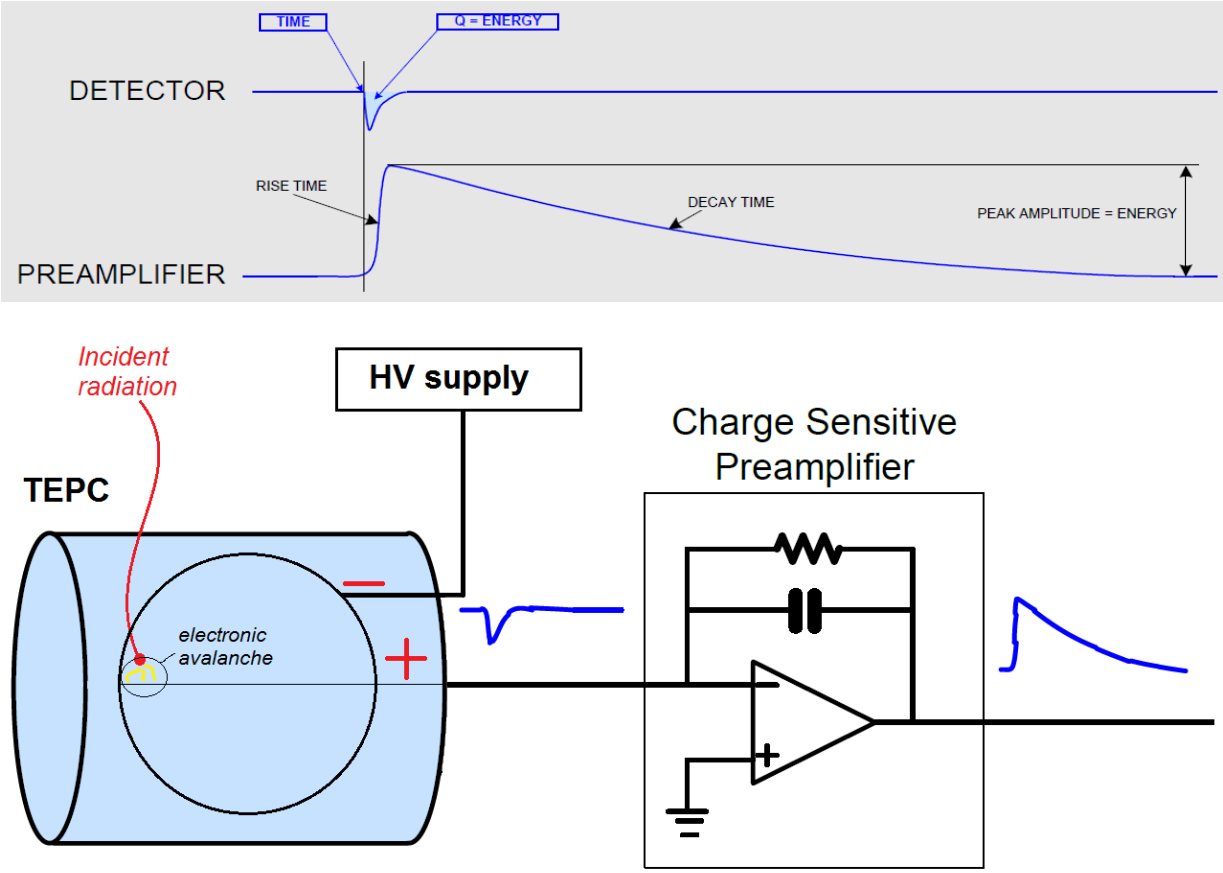

Figure 2.2 - Signal processing from the detector to the output of the Charge Sensitive Preamplifier.

Chap. 4. The acquisition system

Fundamentally, the signal readout from the charge sensitive preamplifier can be achieved in two ways: analogic approach or digital approach.

4.1. Traditional analogic approach

The traditional analog chain for signal readout from nuclear radiation detector usually makes use of almost all-analog chains, where the electronics rely upon four fundamental devices:

- The Charge Sensitive Preamplifier, which integrates the signal coming from the detector converting the negative charge pulse into a voltage step, producing a pulse height which is proportional to the area of the current pulse. In order to have a good charge-amplitude conversion and minimize the noise, the decay time of the output signal must be much larger than the width of the detector signal (due to electronics, the decay time depends from the product *RC* as seen in chapter 3). The long tail makes digitizing the pulse heights impractical, because pulses will often ride on top of the long tail of one or perhaps several preceding pulses (for this reason pile-up of different particles detection can arise). This device is also required in the digital approach.

- The Shaping Amplifier, which provides out a quasi-Gaussian output whose height is still proportional to the energy released by the detected particle. The chain needs this device after the preamplifier in order to avoid too sharp peaks to be detected with the required precision by the Peak Sensing ADC (Analogic to Digital Converter, the component after the shaping amplifier in the chain). In fact the Peak Sensing ADC works better with wider signals and has limits with very fast and high frequency signals (greater than several GHz). The main parameters of this device are the shaping time and the gain.

- The Peak Sensing ADC, which is able to evaluate and digitize the height of the pulses, and filling a histogram with these values, which corresponds to the released *energy spectrum*.

- The discriminator, that is needed to set the thresholds, and then to exclude all those events below a certain level (normally the noise level).

In order to preserve the timing information, the fast component of the signal (rising edge) is usually treated by a Fast Amplifier (or Timing Amplifier) that derives the signal; the output of the fast amplifier usually feeds a chain made out of a

Discriminator followed by a TDC (Time to Digital Converter, a device for recognizing events and providing a digital representation of the time they occurred) and a Scaler for the timing and counting acquisition. Usually the Fast Amplifier is included into the Shaping Amplifier module and the relevant signal is provided as a separate fast output (or timing output). [19]

When a pulse is processed by an analog chain block, the maximum read-out rate is limited by the need to complete the processing of the current pulse before being able to process a successive valid signal. When the processing time of a pulse is larger than the time interval before the arrival of the next pulse, the analog chain is temporarily blind and misses one or more successive pulses. Thus the actual live counting time is smaller than the total counting time, and the difference between total time and live counting time is indicated as “dead time”.[17]

In figure 2.3 the analogic approach chain is shown.

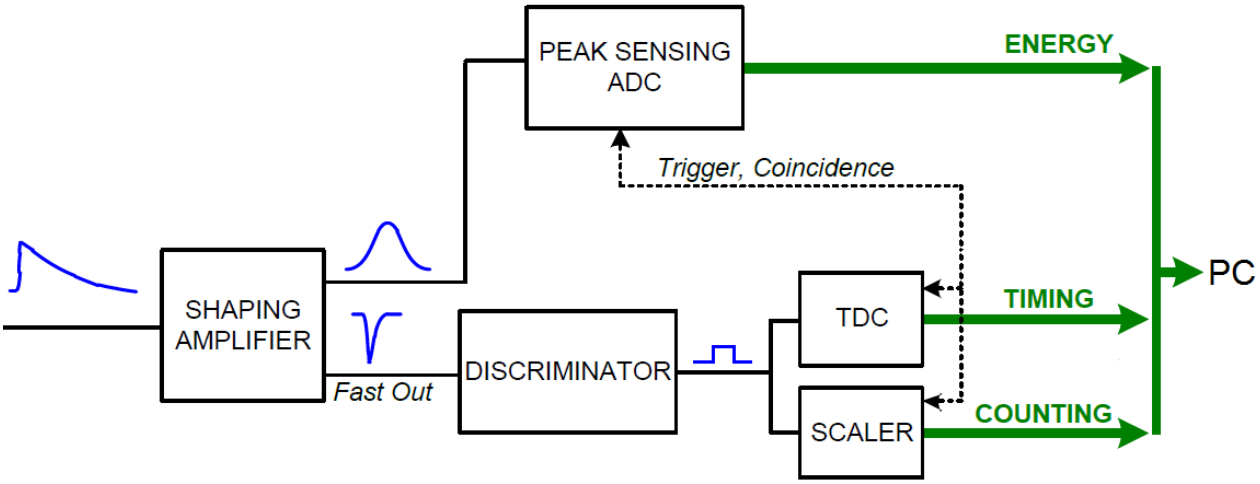

Figure 2.3 - The analogic approach chain.

4.2. Digital approach

The availability of very fast and high precision Flash ADCs (a type of analog-to-digital converter that uses a linear voltage ladder with a comparator at each "rung" of the ladder to compare the input voltage to successive reference voltages) permits to design acquisition systems in which the analogic to digital conversion occurs as close as possible to the detector, so than the preamplifier signals is digitized at the front end of the signal processing chain. The principle of operation of a Waveform Digitizer (Flash ADC) is the same as the digital oscilloscope: when the trigger occurs, a certain number of samples (acquisition window) are saved into one memory buffer. Since in the analog approach we have a network of electrical components connected in series, each element creates a time difference between its input signal and output signal. This leads to a limit in the maximum read-out rate and so to a dead-time, as

discussed in before. In the digital approach, thanks to the Multi Event Memory (a memory able to record successive events at the moment when it is processing the previous), there is no dead-time between the triggers, at least until the readout rate allows the memory buffers to be read and freed on average faster than they are written, thus avoiding the memory to go full. The main advantage of the digital approach is that it is very easy to implement delay lines (it is sufficient to move back the pointer in the memory buffer that contains the samples). Moreover, the digital processing can calculate the baseline of the signal and subtract it (named pedestal cancellation). The high dynamic range is another advantage of the digital approach; in fact, unlike the analog ADC in which the integrating capacitor can saturate, here the charge is represented by the sum of a set of samples (accumulator) and it can be as large as you like just changing the number of bit of the accumulator. [17] [19]

The analogies between the two approaches (digital and analogic) are:

- Both system have a constant “shaping time” and must be calibrated for the pole-zero cancellation circuit, a system able to correct the presence of an undershoot in the shaped pulse (that normally returns very slowly to zero). The pole-zero need to be compensated to be on the baseline level in order to have the correct pulse height. If not, it is possible that the new pulse rides on the undershoot of the old pulse. The result is an amplitude defect and a distortion of the pulse height information in the new signal.

- For both, a long shaping time gives a better resolution but with a higher pile-up probability.

- Both are AC coupled (it means that they allow only alternating current signals to pass through a connection) with respect to the output of the preamplifier whose baseline is hence removed, but both have their own output DC offset and this constitutes another baseline for the peak detection. DC coupling allows both AC (alternating current) and DC (direct current) signals to pass through a connection.

In figure 2.4 a simplification of the general digital approach chain whit a focus on the Flash ADC is shown. DPP is the acronyms for Digital Pulse Processing system.

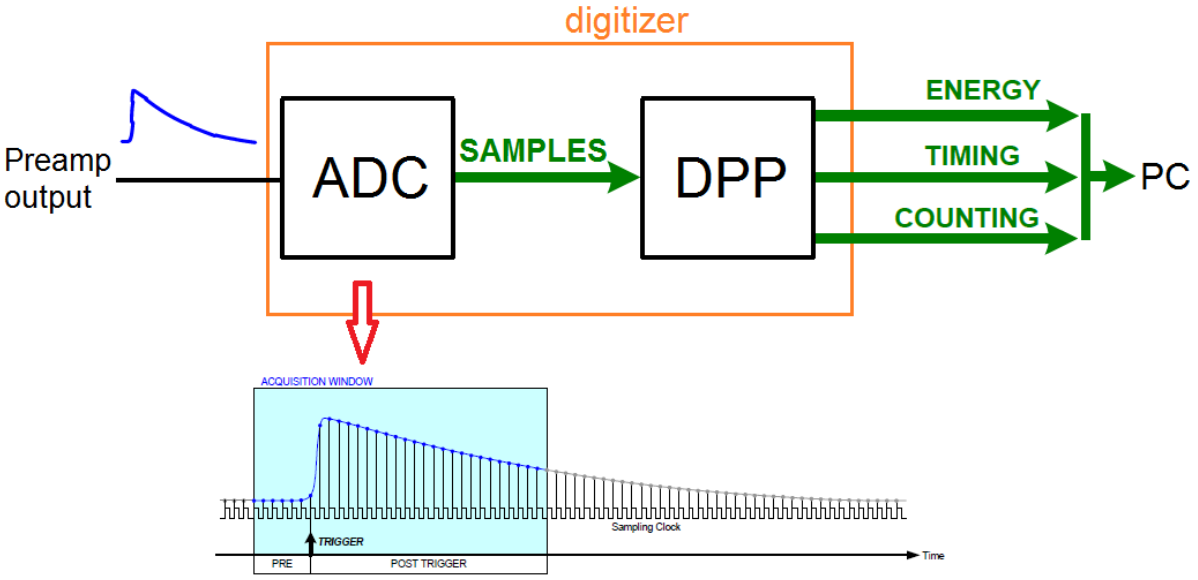

Figure 2.4 – The digital apporoach.

4.2.1. The CAEN DT5780 acquisition system

In figure 2.5 the CAEN DT5780 acquisition system is shown. In the CAEN digital approach all blocks from the shaping amplifier to the PC are synthetized into a single device, the digitizer. In figure 2.7 the block diagram of the CAEN DT5780 is shown.

The first block after the polarity selector is the decimator filter. The effect of this component is to scale down the sampling frequency of a factor (2, 4 or 8), so it can be used in the case the signal is particularly slow. The decimator might have also benefits in terms of noise, since it averages a certain number of samples to make a new sample for the data stream.

After the decimator, there are two parallel branches: one for timing and triggering, the other one for the energy. [18][19]

Figure 2.5 – The CAEN DT5780 acquisition system.

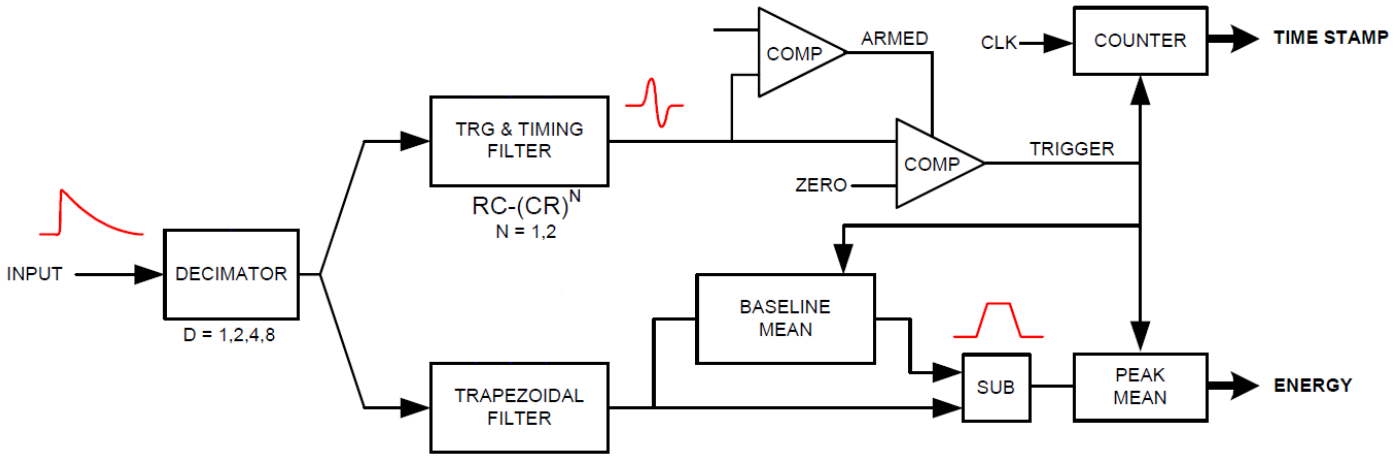

Figure 2.6 – Block diagram for CAEN DT5780.

4.2.1.1. The Trigger and Timing Filter

The aim of the Trigger and Timing Filter (TTF) is to identify the input pulses, generate a trigger on these signals and calculate the time of trigger firing. The user is able to interact with this unit setting some parameters through the software.

The TTF performs a digital RC-CR^2 filter, as shown in figure 2.7.

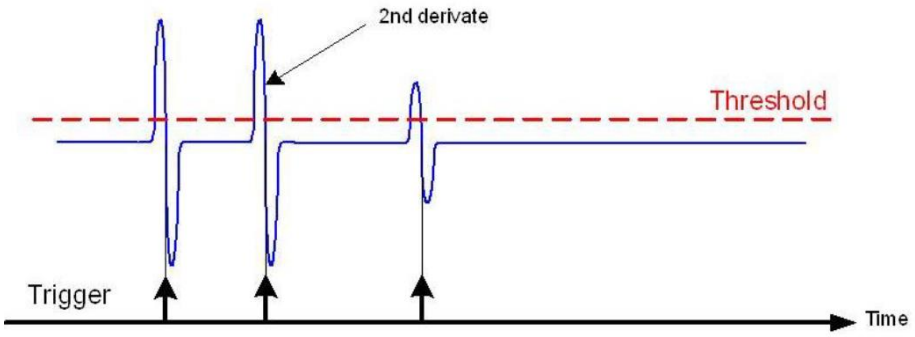

Figure 2.7 – The trigger and timing filter.

The RC-CR^2 filter is bipolar and the zero crossing (independent from the pulse amplitude) corresponds to the trigger firing. The trigger logic gets armed at the threshold crossing, so one parameter that needs to be set is the threshold value, corresponding to set the LLD (lower level discrimination) of the energy spectrum.

The integrative component of the RC-CR^2 is a smoothing filter based on a moving average filter, that reduces the high frequency noise and prevent the trigger logic to generate false triggers on spikes or fast fluctuation of the signals. The derivative component allows subtracting the baseline, so that the trigger threshold is not affected by the low frequency fluctuation. Moreover the pileup effect is significantly reduced. The other parameter that needs to be set for the trigger logic is the RC-CR^2 smoothing, corresponding to the number of samples used for the RC-CR^2 signal formation. Increasing this parameter may help in reducing high frequency noise.

The third parameter in this unit on which we can operate through the software is the Input Rise Time. It is the time in which the RC-CR^2 reaches its maximum value. This value should correspond to the input rise time, in such a way the RC-CR^2 peak value corresponds to the height of the input signal. [19]

4.2.1.2. The Energy Filter (Trapezoidal Filter)

The algorithm implemented in the digitizer is based on a trapezoidal filter called DPP-PHA (Digital Pulse Processing for Pulse Height Analysis). As in the traditional analog chain the Shaping Amplifier is able to convert the signal exponential shape from the Charge Sensitive Preamplifier into a Gaussian shape whose height is proportional to the pulse energy, in the same way the Trapezoidal filter is able to transform it into a trapezoidal signal whose flat top height is proportional to the input pulse height (so to the energy released by the particle in the detector).

Setting the parameters of the trapezoidal filter on the software interface is like operating on the potentiometer (the voltage measurer) of the shaping amplifier. The settings of these parameters will affect the energy resolution and maximum counting rate, so it is fundamental to choose the right compromise between high resolution (high value of trapezoid rise time) and pile-up rejection (and corresponding dead time).

The pile-up rejection is the problem that arises when two pulses are separated by less than the trapezoid duration (that can be calculated as 2 times the Trapezoid Rise Time plus the Trapezoid Flat Top time), then the relevant trapezoids overlap. The Digital MCA read out capability is rather independent from the ADC sampling time and processing speed than from the signal width, and in general allows for higher counting rates than the analog chain. The digital MCA dead time is also an information on the relationship between total measurement time and live counting time values. [19]

In figure 2.8 the evolution of the signal in the digitizer and the settings summarize for both the Trigger and Timing Filter and the Trapezoid Filter are shown.

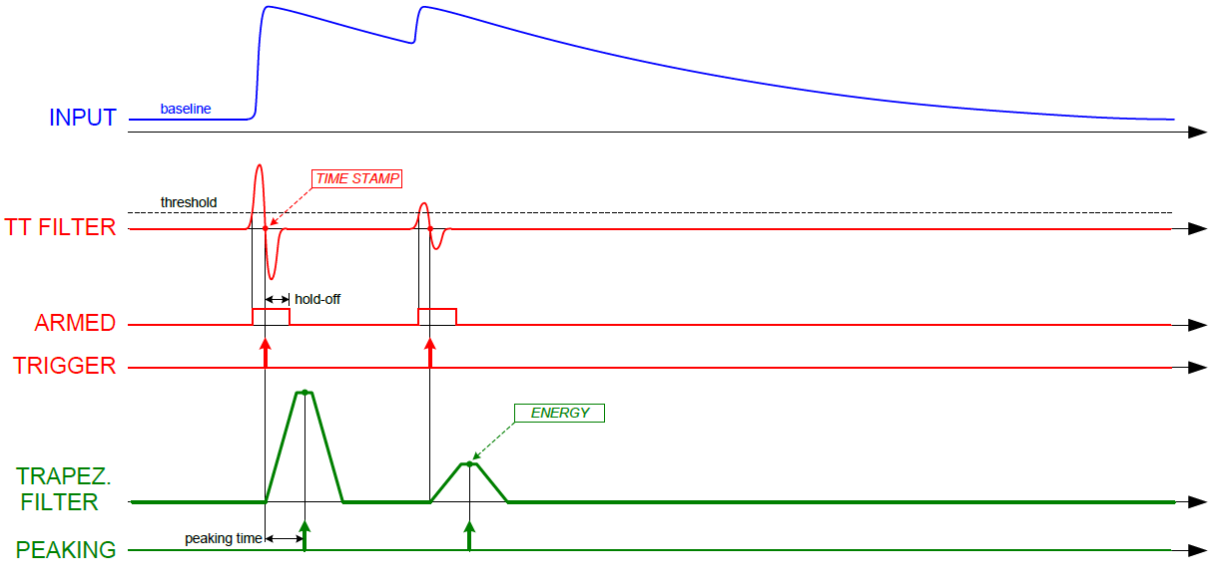

Figure 2.8 - Simplified signals scheme of the Trigger and Timing filter (red) and the Trapezoidal Filter (green).

4.2.2. The Canberra InSpector 2000 acquisition system

In figure 2.9 the Canberra InSpector 2000 acquisition system is shown.

For this device there aren't detailed information about how the signal is processed. It is a sort of "black box" from the point of view of the hardware.

As with the CAEN, the InSpector 2000 has dedicated software that consents to play with some settings.

The digital filter employed has a Triangular/Trapezoidal weighting or shaping function. The processing time (Shaping) is set by the Rise Time and Flat Top selections: the Rise Time sets the noise filtering characteristics of the Digital Filter while the Flat Top allows for the charge collection time of the particular detector. The triangular/trapezoidal shaping function is symmetrical. The fall time cannot be set independently, but it always equals the Rise Time selection. [20]

The shaping times recommended for highest resolution produce a trapezoidal pulse response with a processing time that is equivalent to traditional analog one. Longer rise time and flat top settings provide better noise filtering and reduced ballistic deficit. However, as the system count rate increases, resolution and throughput may degrade as a result of increased processing time and pulse pile-up effects. [20]

At high count rates, Pole/Zero (P/Z) matching adjustment is extremely critical for maintaining good resolution and low peak shift. For precise and optimum setting of the P/Z matching, the digital oscilloscope can be used.

Another setting that needs to be cited is the Fast Discriminator threshold mode (FDisc):

- AUTO - allows the threshold to be optimized automatically above the system noise level;
- MANUAL - allows the threshold to be manually adjusted.

To set the threshold value the key parameter is the LLD. Automatic or Manual LLD mode can be selected;

- AUTOMATIC - the LLD cutoff is automatically set just above the spectral noise threshold;
- MANUAL - allows the LLD cutoff to be set manually as a percentage of the full scale spectral size or range.

Figure 2.9 – The Canberra InSpector 2000 acquisition system.

Experimental setup

Chap. 5. The charge sensitive preamplifier evaluation

During this work we evaluated and used three different preamps, one manufactured by Canberra (Model 2006 SS-CSP0158), one by Ortec (Model 142PC) and one specifically created from SCK to be used with TEPC LETSW5, which has been modified in the course of this study to improve his performances. In Figure 3.1 a picture of the three preamplifiers is shown. The schemes of the different preamplifiers are shown in Appendix A.

Figure 3.1 - Picture and scheme of the three preamplifiers. a) Canberra preamp, b) SCK preamp, c) Ortec preamp.

First of all we have checked which of the three preamplifiers has a better performance in terms of electronic noise, amplification and characteristics time. To this purpose, we tested the preamplifiers with a precision pulser (Figure 3.2), simulating the TEPC pulse of the internal alpha source, in order to compare the output signal of the preamplifiers with the same initial signal charge. To replicate the conditions of the output signal of the TEPC (and so to have a current pulse, not a voltage pulse), we needed a resistor upstream the input of the two preamplifiers. The resistor value is 1 [GΩ] and it is shown in Figure 3.3. In order to see the signal we used the oscilloscope in Figure 3.4. In table 3.1 the results obtained for the three different preamplifiers are shown.

Figure 3.2 – Pulser.

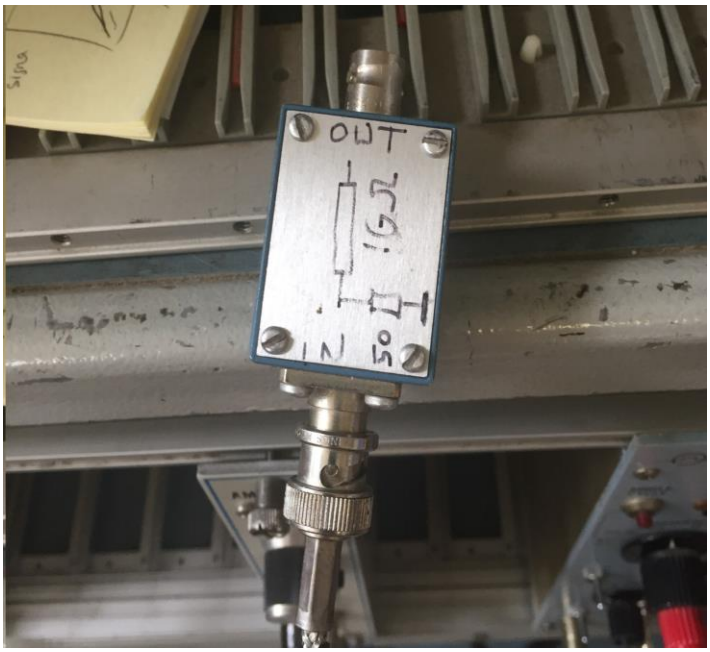

Figure 3.3 – Resistor.

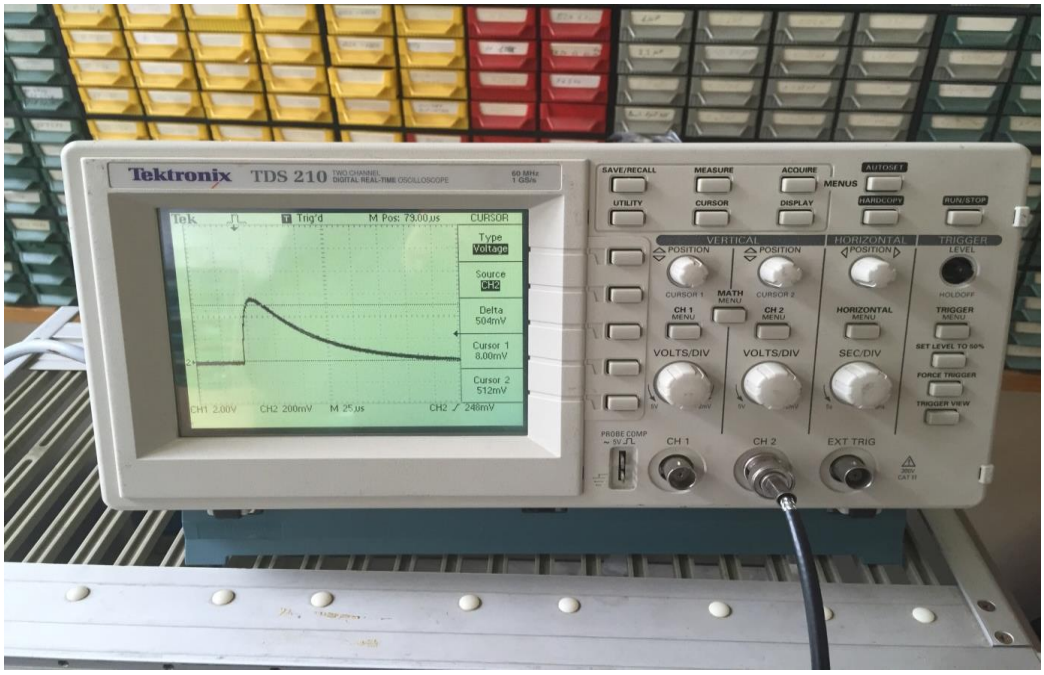

Figure 3.4 – Oscilloscope.

Table 3.1 – Results obtained by simulating the signal of the internal Alpha source.

	Canberra	**SCK v1.0**	**Ortec**	**SCK v2.0**
Simulated input voltage (TEPC gain) (V)	700	700	700	700
Rise time (µs)	8	20	8	8
Fall time (µs)	250	1250	500	500
Pulse height (mV)	300	2300	1920	1300 mV
Noise level (mV)	4	25	10	20

As all the measurements were taken at the same simulated input voltage, the ratio between the pulse heights is the same as the ratio between the gains of the preamplifiers.

The ideal preamplifier for this work should have ‘rise time’, ‘fall time’ and ‘noise level’ parameters as low as possible and pulse height parameter as large as possible. From the results shown in the table seems that the two preamplifiers with the better compromise between these parameters are the ones from Ortec and SCK (version 2.0). Since the Ortec preamplifier has the lower noise level, it was the chosen one for the more critic measurements (i.e. the measurements in BR1 reactor channel).

Chap. 6. The optimized electronic chain

The theoretical signal processing electronic chain can be schematically represented as in figure 3.5. Thanks to the external oscilloscope, we were able to detect some noise and electronic problems that were influencing our acquisition. To fix these problems, we applied some changes to the electronic chain. Due to the design and scheme of the SCK preamplifier this devices are not needed in the configurations that include it (this because the way in which the box of this preamplifier is structured manages to avoid the interference of eddy currents). At first, we introduced a capacitor to fix an offset problem on the data output of the charge sensitive preamplifier (Figure 3.6). The capacity is *2.2* pF.

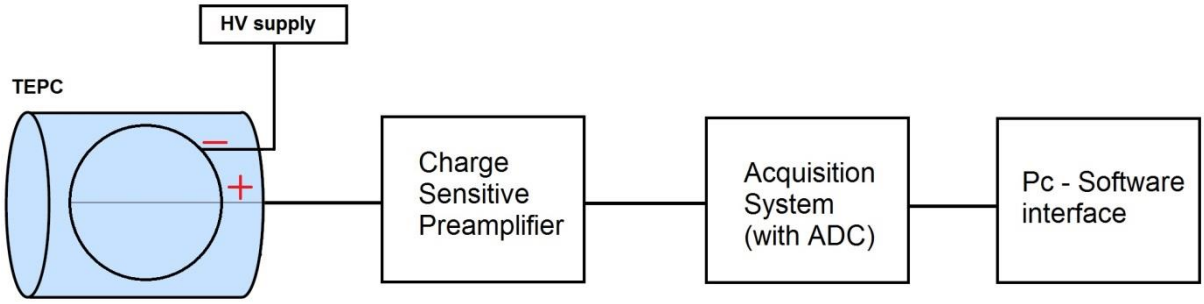

Figure 3.5 – The theoretical electronic chain for the signal acquisition.

Figure 3.6 – Capacitor.

The second correction applied is a filter applied on the high voltage cable able to restrict an high frequency noise problem. In Figure 3.7 the high frequency noise filter is shown. Still on the high voltage cable, between the high frequency noise filter and the TEPC high voltage connector, we had to introduce another filter (a magnetic filter) to remove a spikes carrying problem (Figure 3.8).

Figure 3.7 – High frequency noise filter.

Figure 3.8 – Spikes remover magnetic filter.

The last device we added is a closed wire connected to the HV input of the preamp (to set the 'earth', Figure 3.9). Actually this aid is needed just in the configurations that include the Canberra preamplifier. In figure 3.10 the final block diagram of the electronic chain is shown.

In figure 3.11 and figure 3.12 the final acquisition setups with Ortec preamplifier for both InSpector 2000 and CAEN DT5780 acquisition systems are shown.

Figura 3.9 – Closed wire.

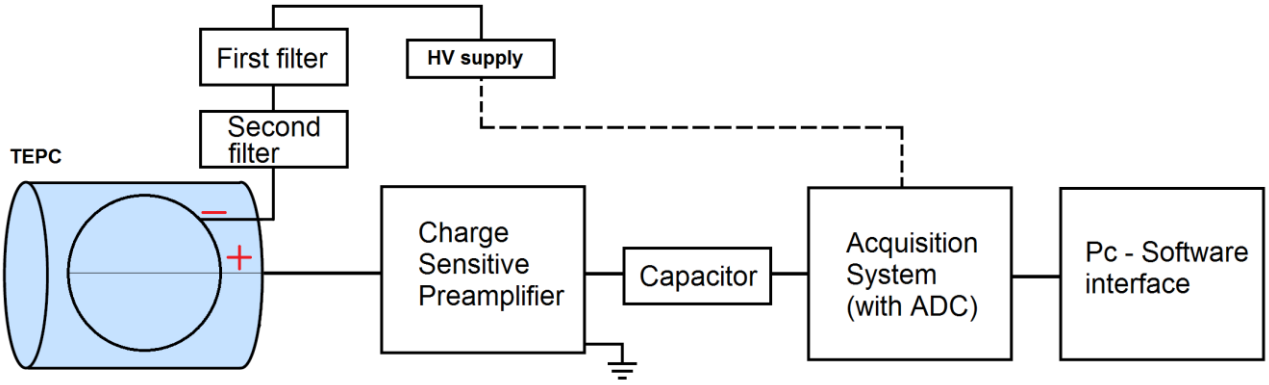

Figure 3.10 – Complete block diagram of the electronic chain.

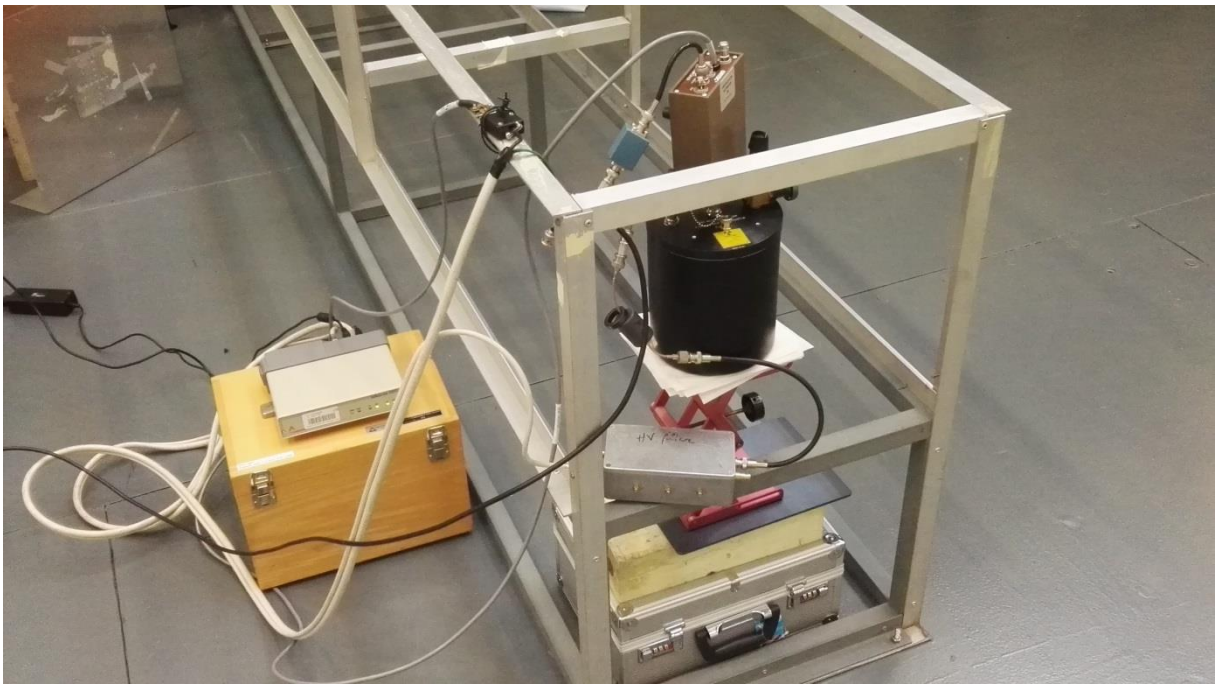

Figure 3.11 - Final acquisition setup with Ortec preamplifier and acquisition system InSpector 2000.

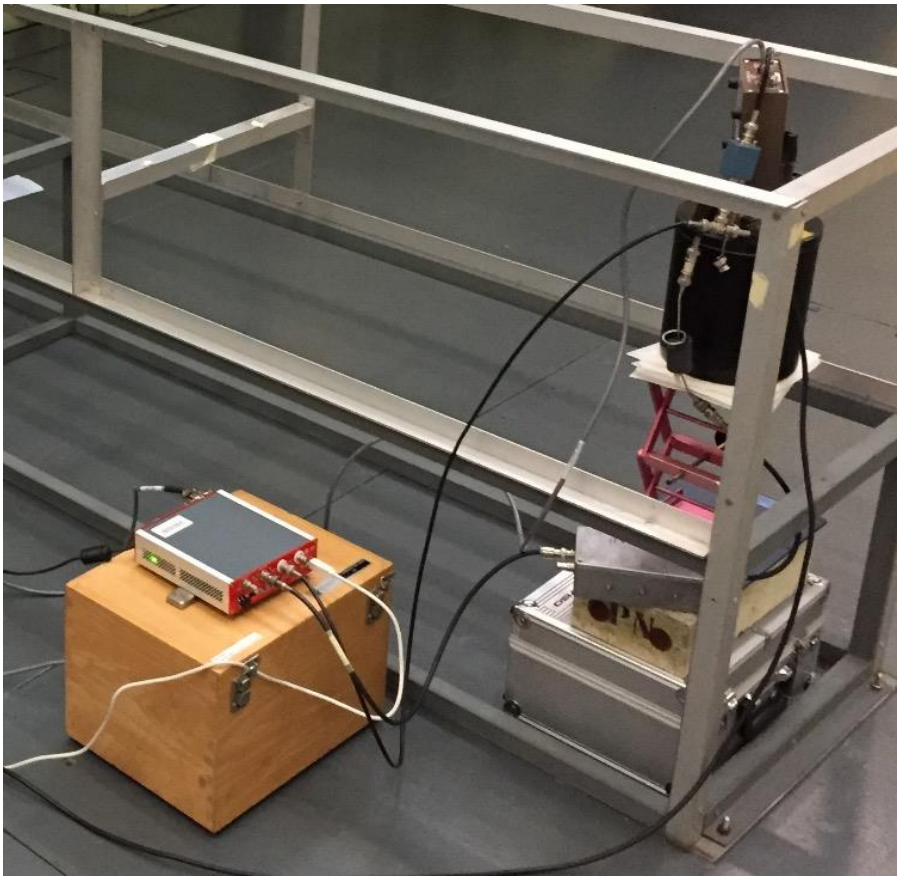

Figure 3.12 - Final acquisition setup with Ortec preamplifier and acquisition system CAEN DT5780.

Chap. 7. The background problem

Checking with the external oscilloscope we realized that our TEPC was measuring some abnormal signals. We have ruled out the possibility to have other sources in the room, so we checked the TEPC with X-rays in order to see if there was any internal physical damage. In figure 3.13 an X-ray image of the TEPC is shown. We concluded that these abnormal signals could be due to three causes: an interference of the internal alpha source for calibration due to a malfunction of the mechanism to turn it on-off, a gas degradation (we performed a refilling procedure and we excluded this cause) or to a malfunction of the central anode.

Since the frequency of these background signals doesn't change if we are irradiating the device has been decided, to prevent these signals from affecting our measurements, to subtract a previously measured background.

In figure 3.14 an example of the background measured by the SCK preamplifier and Inspector acquisition system is shown.

In table 3.2 the settings used to take this measurement are shown.

Table 3.2 – Settings used to measure the background.

Rise Time	4.8 μs
Flat Top	1.0 μs
BLR Mode	Medium
Pole 0	666
Gain	2.5x
FDISC	Manual, 2.0%
LLD	Manual, 0.2%

Of course, we had to subtract from each measurement the specific background measured in the particular acquisition setup configuration.

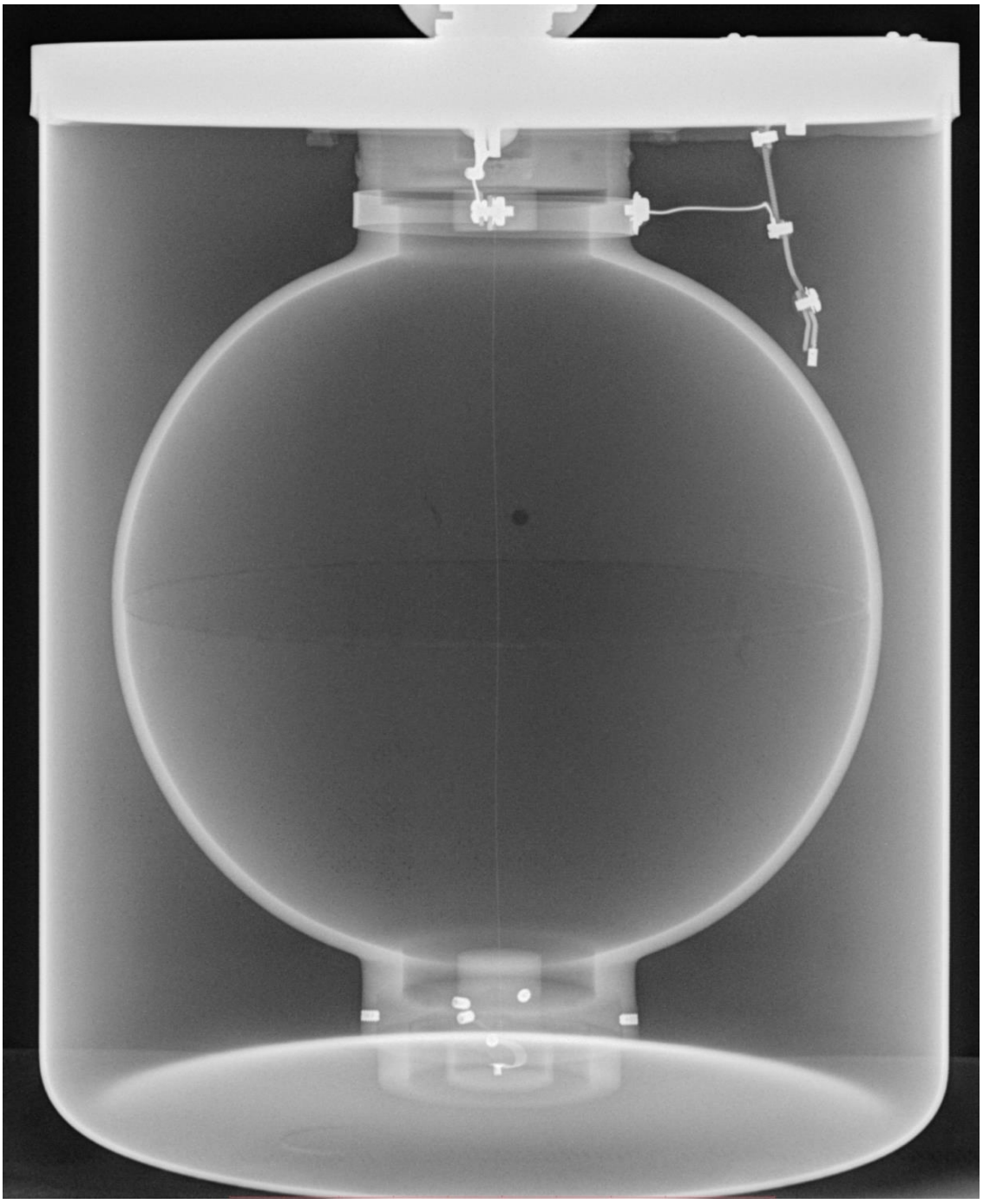

Figure 3.13 – X-ray image of the TEPC. The source in this position is switched off.

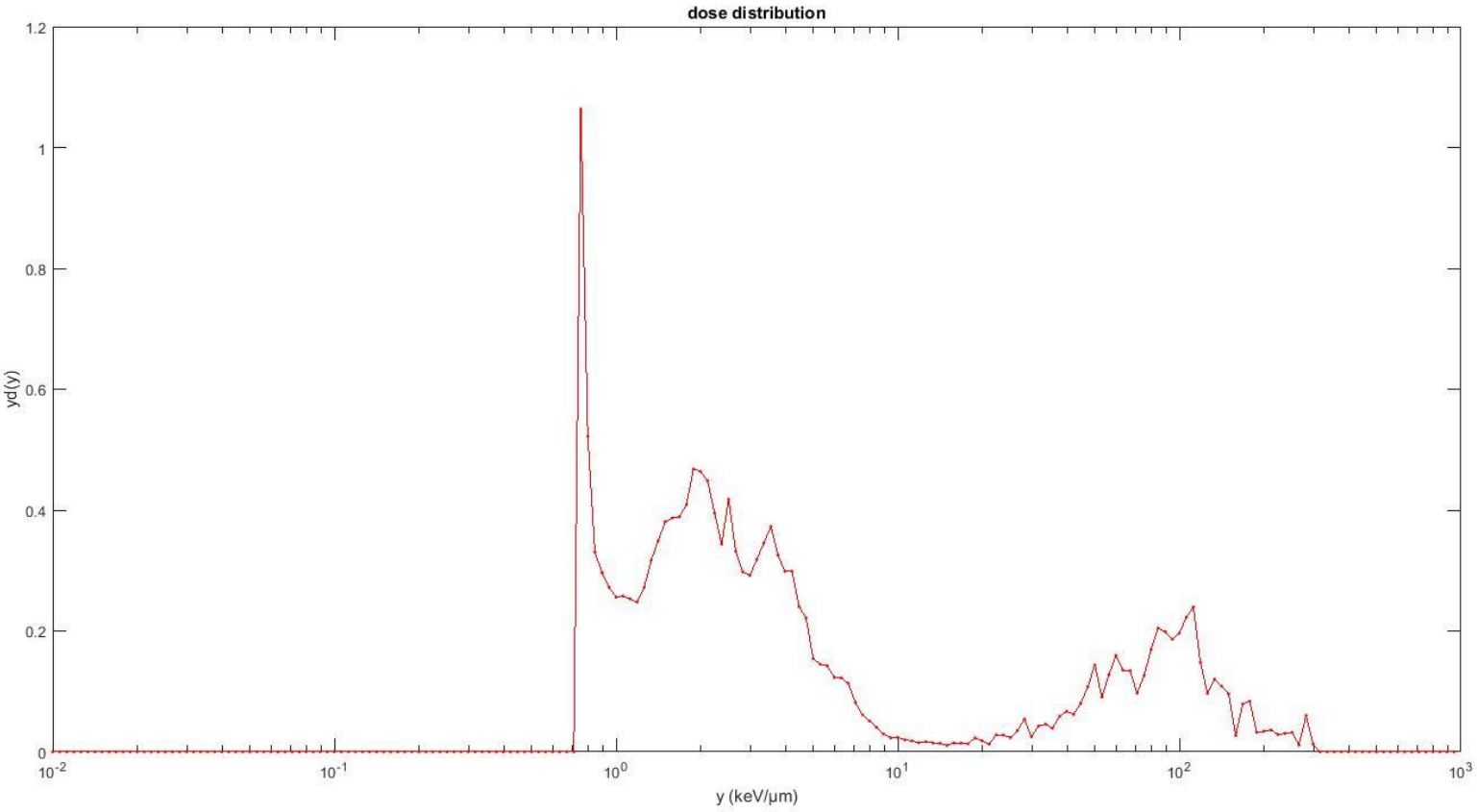

Figure 3.14 - Microdosimetric distribution yd(y) vs. y for the background measured with SCK preamplifier and Inspector acquisition-system.

Measurement report

Chap. 8. Linearity tests

We performed measurements in:

- Gamma ^{137}Cs field
- Gamma ^{60}Co field
- Mixed gamma-neutron ^{252}Cf field
- Mixed gamma-neutron at the z55 channel in Belgian Reactor 1 (BR1). BR1 is an air-cooled graphite reactor that runs on natural uranium. [24]

On the TEPC, the only parameter you can easily play with is the voltage. This parameter affect the gain on the output signal to the preamp and must be in a determined range, so to have the operation of the detector as a real tissue equivalent proportional counter. The range depends from the tissue equivalent gas composition and from the gas pressure, and so it can change in the meantime between two fillings of the TEPC. The voltage to be applied to the TEPC shall be imposed by the acquisition system software. We used three different software to control the acquisition process, one for the Inspector Canberra 2000 and two different specific software (an old stably working version and the new one, that needed to be tested) for the CAEN.

As explained in paragraph 4.2, with the CAEN new acquisition system we can play with a lot of parameters, which in the specific software have been divided into three groups:

- Input signal parameters; the input dynamic range (which is the maximum output voltage value from the preamp detectable by the acquisition system) the decimator and the digital gain.
- Trigger parameters; the input rise time, the trigger hold off (the minimum time that must elapse between two triggering signals) and the threshold level (the minimum pulse height that must be recorded).
- Filter parameters; the trapezoidal rise time, the decay time, the trapezoidal flat top and the trapezoidal gain.

In order to characterize the new CAEN acquisition system and to achieve the perfect balance between all these settings we did a large number of measurements. Here will be reported only those that have produced the most significant results. Before using the acquisition systems with the TEPC, we needed to check the linearity of our acquisition system configurations. To do this we used a pulser (fig. 3.2) in order to simulate a stable signal of different amplitudes. The results are shown in the next pages.

8.1. SCK Preamp - Inspector 2000

In figure 4.1 and table 4.1 the linearity test values and results for the SCK preamp – Inspector acquisition chain are shown. In table 4.2 the settings used to take these measurements are shown. The values obtained demonstrate the linearity of the acquisition system.

Table 4.1 – Acquisition chain SCK preamp – Inspector linearity test values

Preamp SCK - Inspector		
PreOutput [mV]	Channel	Output preamp/Channel
244	426	0,57
400	764	0,52
544	1050	0,52
720	1412	0,51
1080	2023	0,53
1540	2948	0,52
2400	4570	0,52
3000	5806	0,52
3500	7023	0,50
4240	7963	0,53

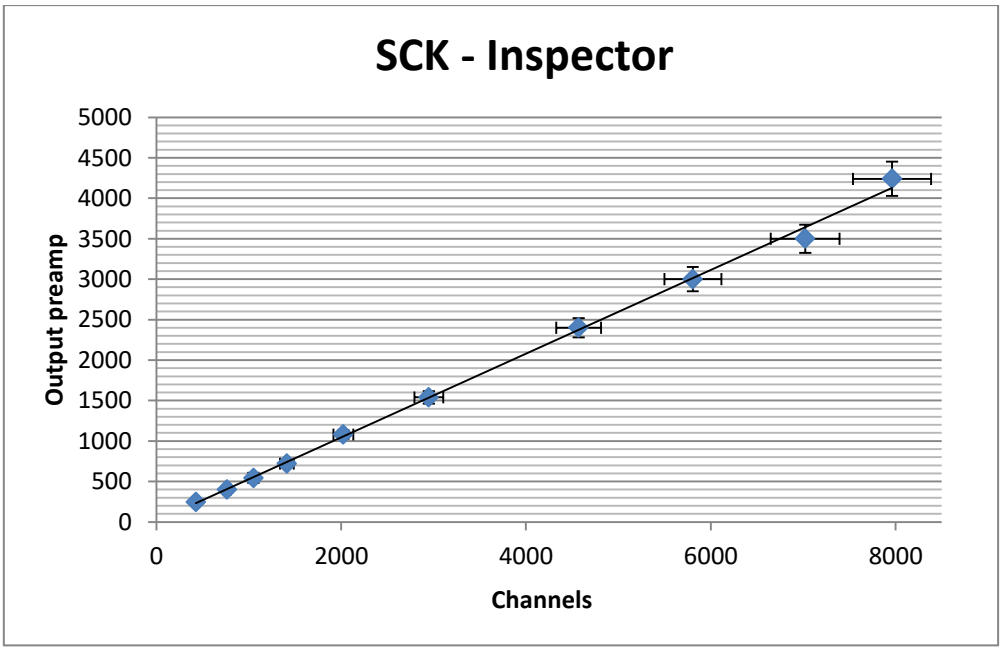

Figure 4.1 - Acquisition chain SCK preamp – Inspector linearity test results

Table 4.2 – Acquisition chain SCK preamp – Inspector linearity test settings

Rise Time	4.8 μs
Flat Top	0.8 μs
BLR Mode	auto
Pole 0	666
Gain	2.5x
FDISC	Manual, 2.0%
LLD	Manual, 0.3%

8.2. Preamp Canberra – Inspector 2000

In figure 4.2 and table 4.3 the linearity test values and results for the Canberra preamp – Inspector acquisition chain are shown. In table 4.4 the settings used to take these measurements are shown. The values obtained demonstrate the linearity of the acquisition system.

Table 4.3 – Acquisition chain Canberra preamp – Inspector linearity test values

Preamp Canberra - Inspector		
PreOutput [mV]	Channel	Output preamp/Channel
74	595	0,12
150	1260	0,12
244	1970	0,12
400	3252	0,12
500	4043	0,12
720	6022	0,12

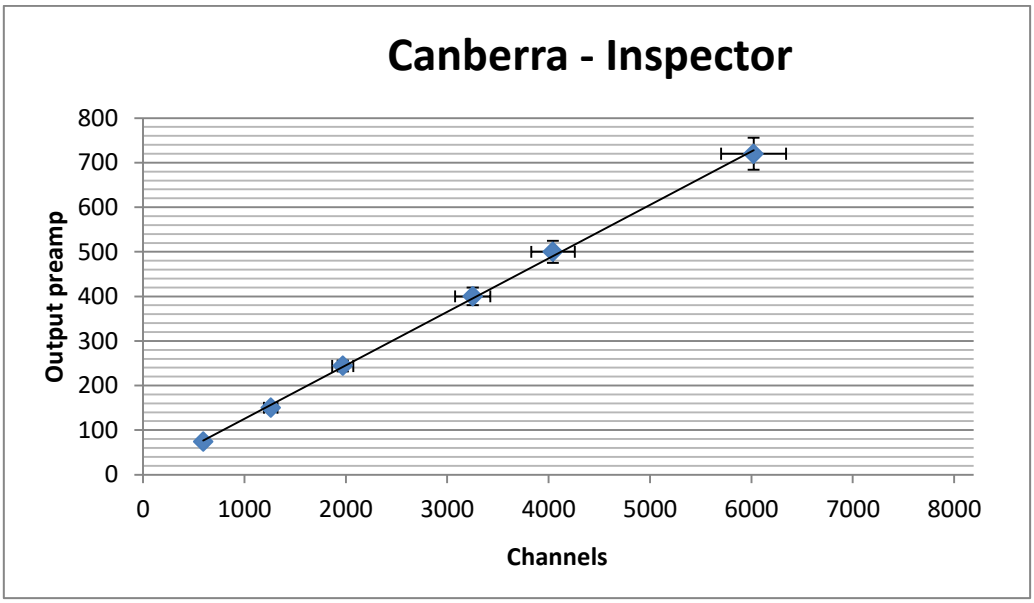

Figure 4.2 - Acquisition chain Canberra preamp – Inspector linearity test results.

Table 4.4 – Acquisition chain Canberra preamp – Inspector linearity test settings

Rise Time	4.8 µs
Flat Top	0.8 µs
BLR Mode	auto
Pole 0	666
Gain	10x
FDISC	Manual, 2.0%
LLD	Manual, 0.4%

8.3. Preamp SCK – CAEN

In figure 4.3 and table 4.5 the linearity test values and results for the SCK preamp – CAEN acquisition chain are shown. In table 4.6 the settings used to take these measurements are shown. The values obtained demonstrate the linearity of the acquisition system.

Table 4.5 – Acquisition chain SCK preamp – CAEN linearity test values

Preamp SCK - CAEN		
Output Preamp (mV)	Channel	Channel/output
60	685	11,42
150	1800	12,00
350	4290	12,26
500	6102	12,20
600	7365	12,27
700	8745	12,49
800	9910	12,39
900	11200	12,44
1000	12335	12,33
1140	13860	12,16
1320	16305	12,35

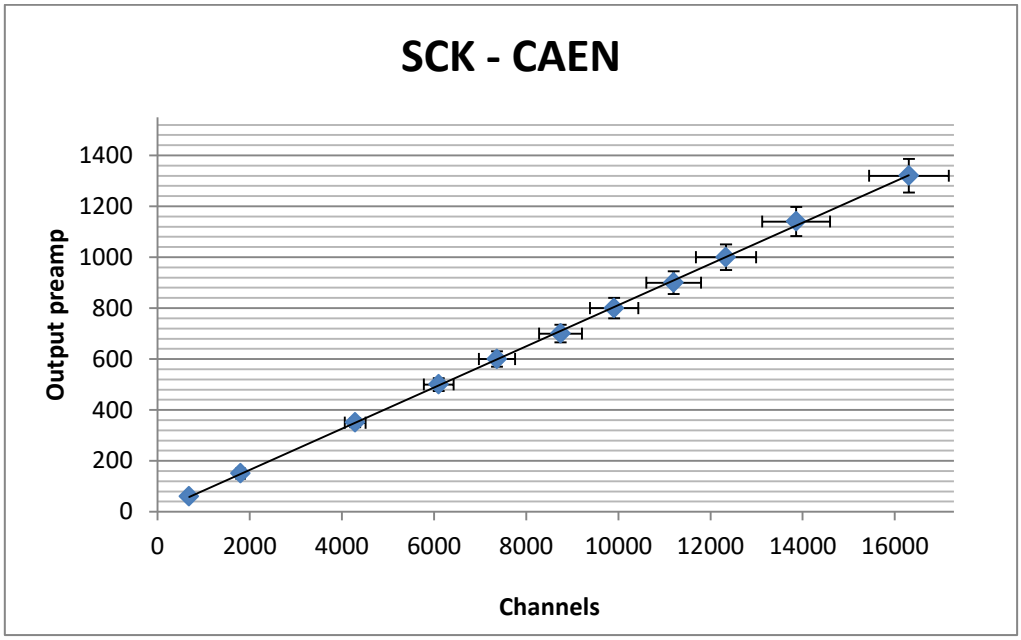

Figure 4.3 - Acquisition chain SCK preamp – CAEN linearity test results

Table 4.6 – Acquisition chain SCK preamp – CAEN linearity test settings

Dynamic Range	1.4 Vpp
Decimator	8
Digital Gain	1
Input Rise Time	6.6 μs
Trigger Hold Off	40 μs
Threshold	160 LSB
Trapezoidal Rise Time	10 μs
Trapezoidal Decay Time	115 μs
Trapezoidal Flat Top	40 μs
Trapezoidal Gain	1

8.4. Preamp Canberra – CAEN A.S.

In figure 4.4 and table 4.7 the linearity test values and results for the Canberra preamp – CAEN acquisition chain are shown. In table 4.8 the settings used to take these measurements are shown. The values obtained demonstrate the linearity of the acquisition system.

Table 4.7 – Acquisition chain Canberra preamp – CAEN linearity test values

Canberra Preamp - CAEN		
Output Preamp (mV)	Channel	Rapporto Channel/Output
30	353	11,77
50	621	12,42
75	925	12,33
150	1889	12,59
300	3790	12,63
380	4847	12,75
600	7510	12,52
900	11701	13,00
1200	15026	12,52
1260	16240	12,89

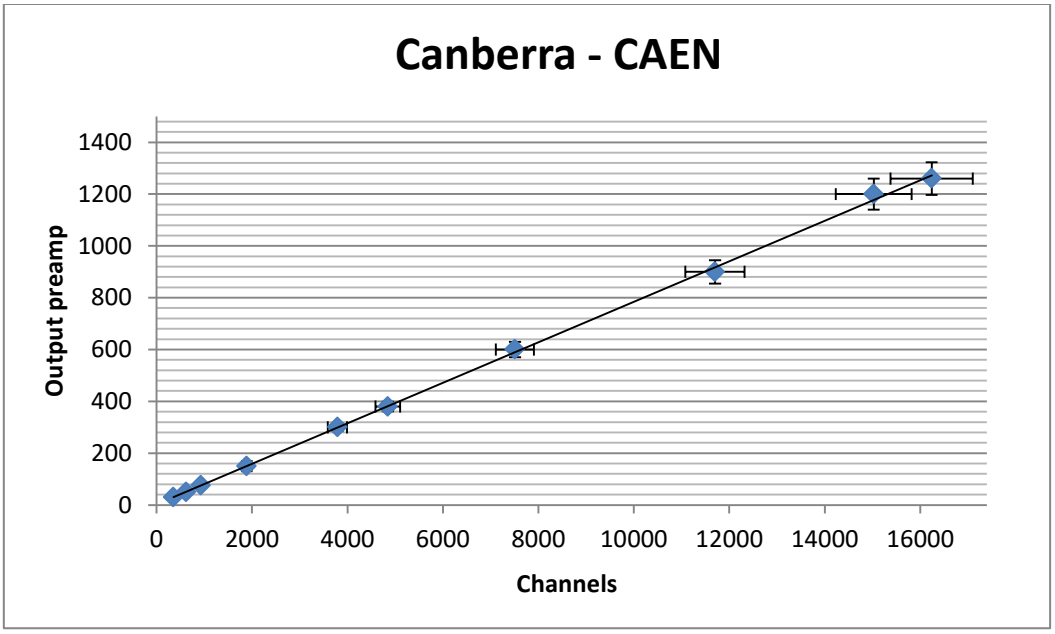

Figure 4.4 - Acquisition chain Canberra preamp – CAEN linearity test results

Table 4.8 – Acquisition chain Canberra preamp – CAEN linearity test settings

Dynamic Range	1.4 Vpp
Decimator	8
Digital Gain	1
Input Rise Time	6.6 μs
Trigger Hold Off	1.3 μs
Threshold	50 LSB
Trapezoidal Rise Time	8 μs
Trapezoidal Decay Time	70 μs
Trapezoidal Flat Top	20 μs
Trapezoidal Gain	1

8.5. Preamp Ortec – CAEN

In figure 4.5 and table 4.9 the linearity test values and results for the Ortec preamp – CAEN acquisition chain are shown. In table 4.10 the settings used to take these measurements are shown.

Table 4.9 – Acquisition chain Ortec preamp – CAEN linearity test values

Preamp Ortec - CAEN		
Output Preamp (mV)	Channel	Channel/output
8	39	4,87
15	76	5,07
20	102	5,10
30	150	5,00
46	227	4,93
78	385	4,94
120	576	4,80
190	927	4,88
276	1364	4,94
352	1718	4,88
428	2119	4,95
504	2499	4,96
656	3121	4,76
1000	4941	4,94
1360	6410	4,71
1700	8254	4,85
2360	11514	4,88
2740	13525	4,94
3240	15601	4,81
3400	16348	4,81

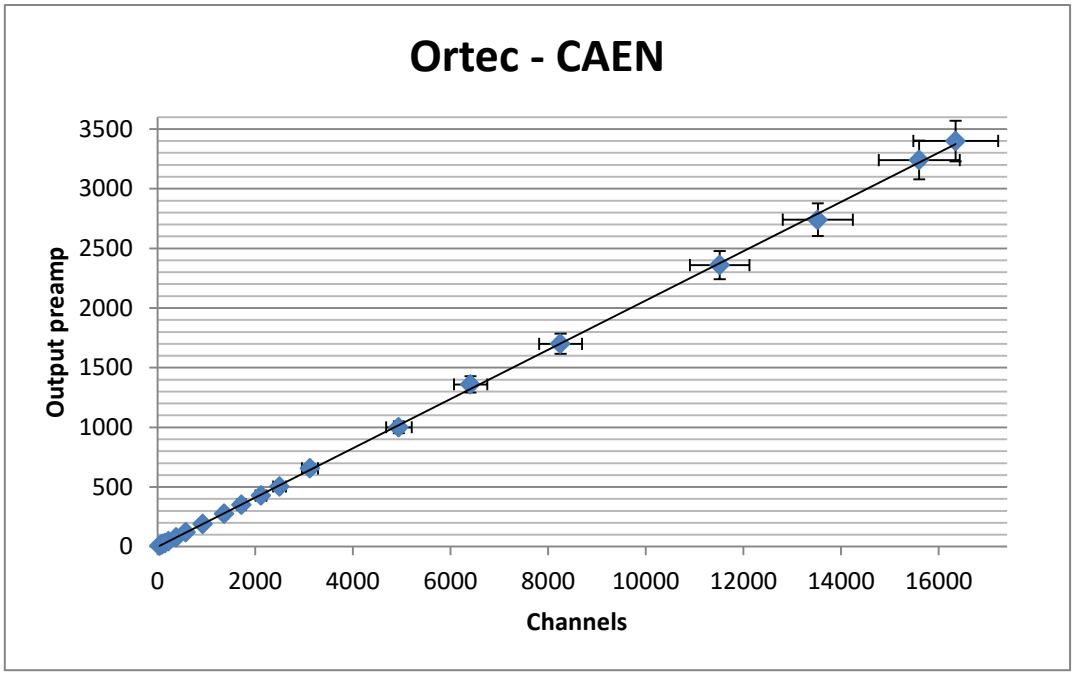

Figure 4.5 - Acquisition chain Ortec preamp – CAEN linearity test results

Table 4.10 – Acquisition chain Ortec preamp – CAEN linearity test settings

Dynamic Range	3.7 Vpp
Decimator	8
Digital Gain	1
Input Rise Time	6.6 µs
Trigger Hold Off	1.3 µs
Threshold	35 LSB
Trapezoidal Rise Time	6.8 µs
Trapezoidal Decay Time	70 µs
Trapezoidal Flat Top	18.20 µs
Trapezoidal Gain	1

The values obtained demonstrate the linearity of the acquisition system.

As we saw in Chapter 3 all the considered settings are subject to more or less important changes depending on the preamplifier used. From the data collected during these tests we found the following acquisition configurations:

- Ortec preamplifier – CAEN acquisition system
- SCK preamplifier – Inspector acquisition system

This two configurations turn out to be the best choice for our purpose.

Chap. 9. Irradiation test results

9.1. ^{137}Cs irradiations

The measurements performed in a gamma source (^{137}Cs) are shown below. These measurements were taken with the SCK preamp and the Inspector acquisition system with an applied voltage of 750 V and a coarse gain of 5. The dose rates we used were 0.1 mSv/h, 0.5 mSv/h, 0.75mSv/h and 1.0 mSv/h. In Figure 4.6 the microdosimetric distribution yd(y) *vs*. lineal energy y is shown.

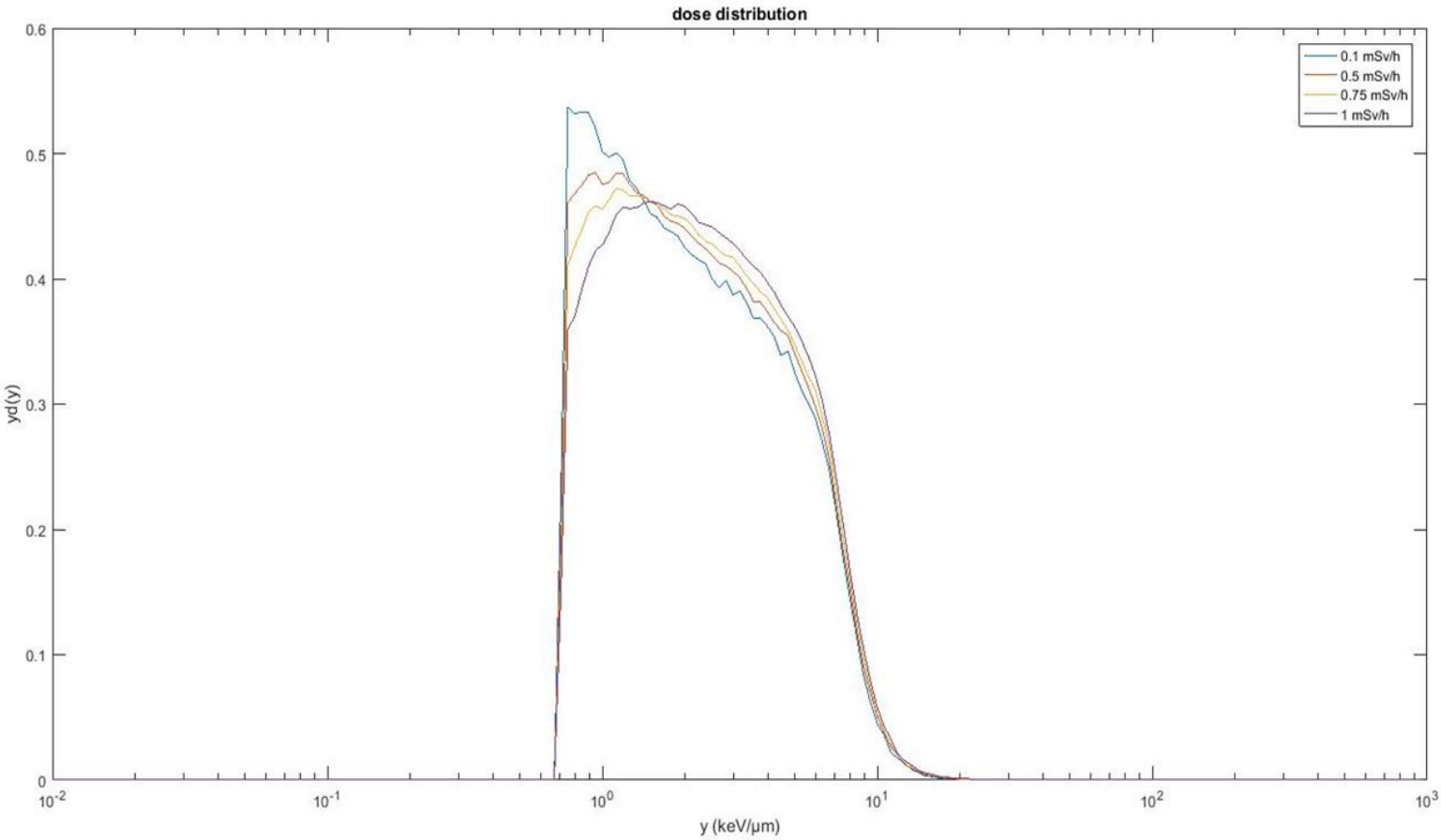

Figure 4.6 – Microdosimetric distribution yd(y) vs. y for ^{137}Cs radiation.

In table 4.11 the settings used to take these measurements are shown.

Table 4.11 - Settings

Rise Time	4.8 µs
Flat Top	0.8 µs
BLR Mode	auto
Pole 0	666
Gain	5x
FDISC	Manual, 2.0%
LLD	Manual, 0.6%

The data have been cut at 0.*7 keV/µm* to avoid the noise.

The measurements performed in a gamma source (^{137}Cs) are shown below. These measurements were taken with Canberra preamp and Inspector acquisition system with an applied voltage of 750V and a coarse gain of 5. The dose rate we used were 0.1 mSv/h, 0.5 mSv/h, 0.75mSv/h and 1.0 mSv/h. In Figure 4.7 is shown microdosimetric distribution yd(y) *vs*. lineal energy y.

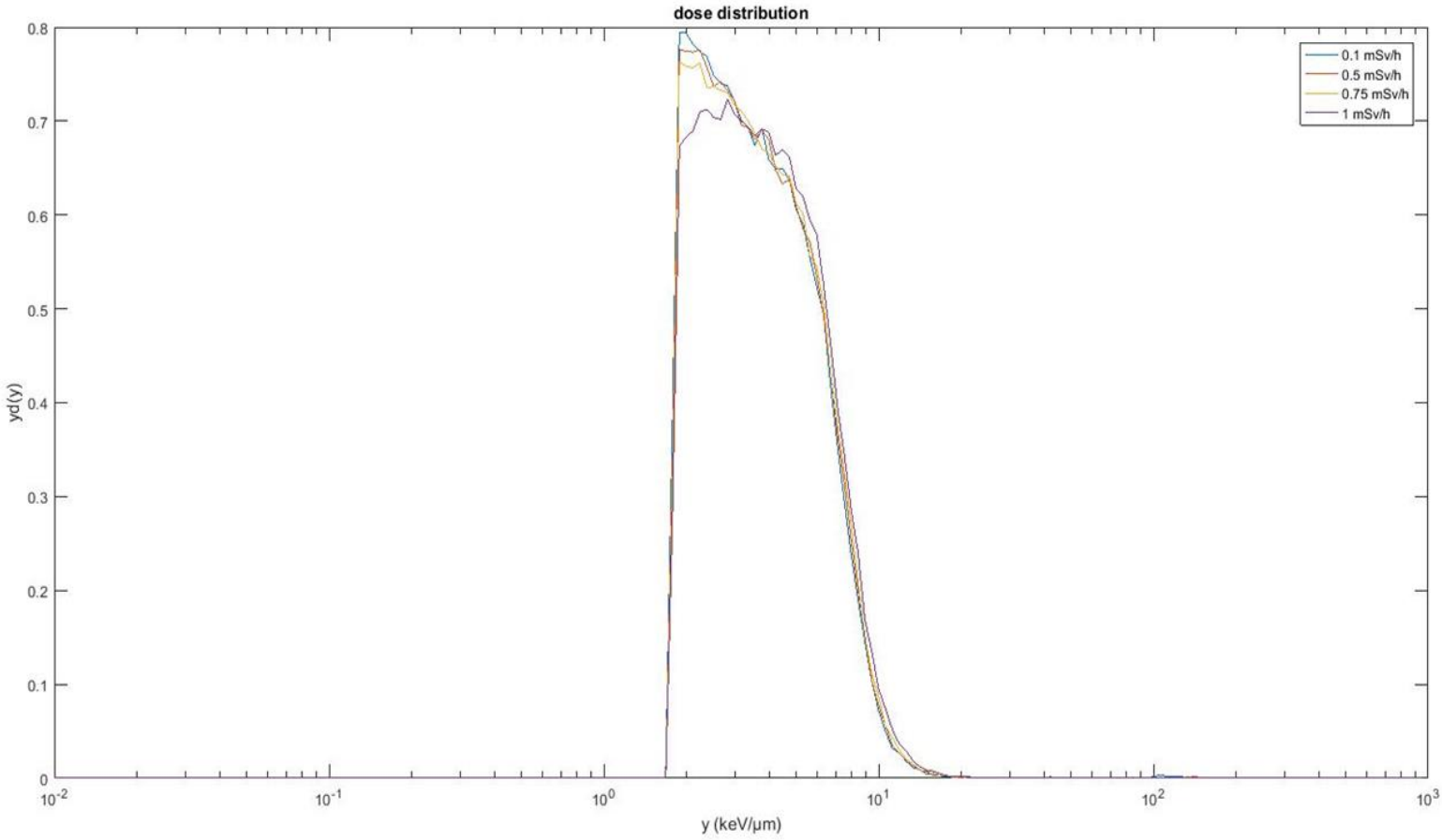

Figure 4.7 - Microdosimetric distribution yd(y) vs. y for ^{137}Cs radiation at different dose rates.

.

In table 4.12 the settings used to take these measurements are shown.

Table 4.12 - Settings

Rise Time	4.8 μs
Flat Top	0.8 μs
BLR Mode	auto
Pole 0	666
Gain	5x
FDISC	Manual, 2.0%
LLD	Manual, 0.3%

The data have been cut at *1.7 keV/μm* to avoid the noise.

In Figure 4.8 is shown a comparison between the dose distribution measured with the two different preamplifiers, Canberra (test1) and SCK (test2) at the same voltage and coarse gain by Inspector acquisition system.

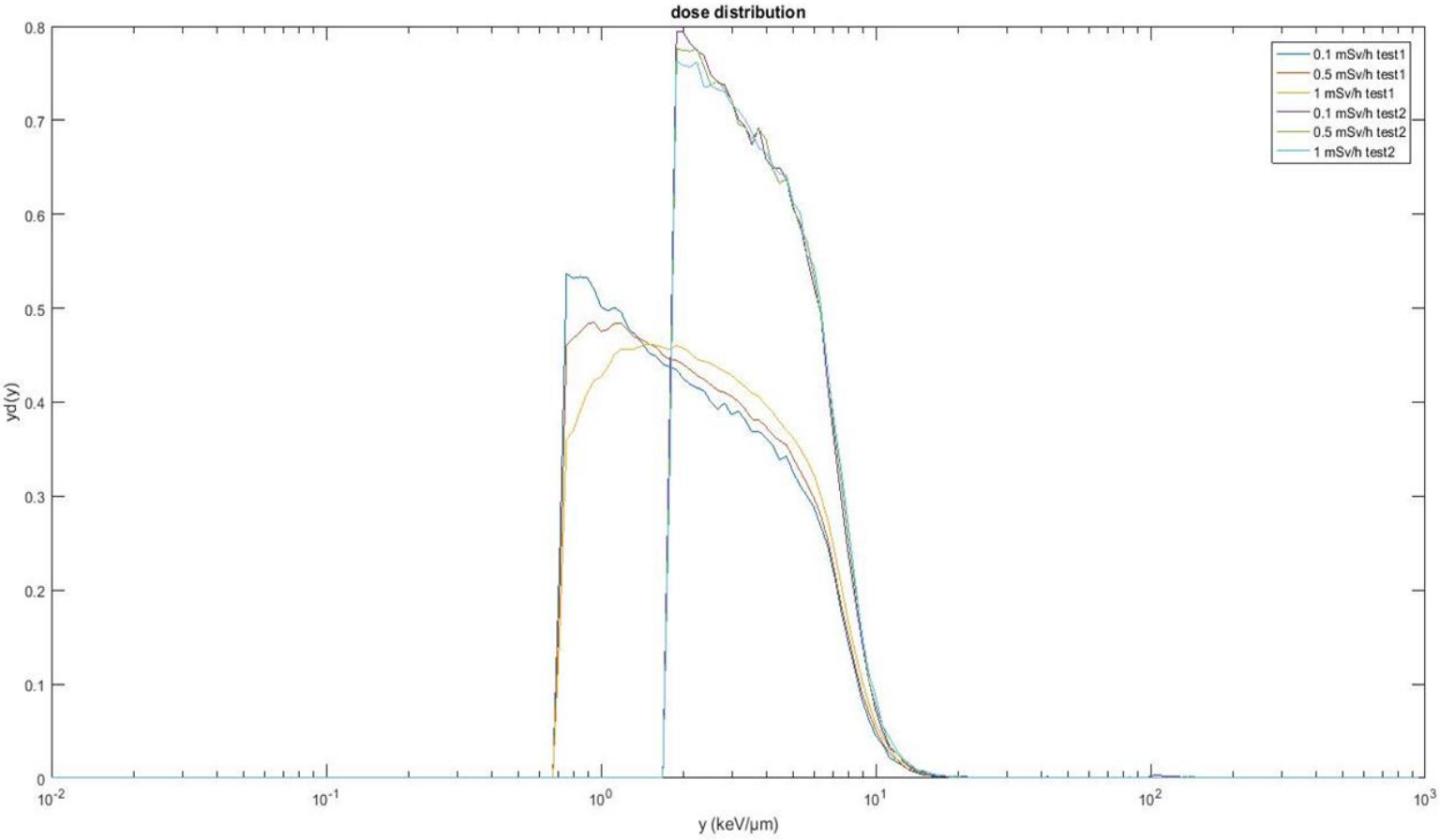

Figure 4.8 - Comparison between the dose distribution measured for a ^{137}Cs source with the two different preamplifiers (Canberra-SCK).

From both these measurements can be seen how increasing the dose rate we may encounter pile-up problems. In fact, in the low-lineal energy region some signals are added to each other, this leads to a spectrum distortion with a trend of dose distribution which varies with the dose rate variation. These could be due directly to a physical limit of the TEPC or to a slowness in the acquisition of the signal from the electronic chain.

9.2. ^{60}Co irradiations

The measurements performed in a gamma source (^{60}Co) are shown below. These measurements were taken with SCK preamp and Inspector acquisition system with an applied voltage of 750V and a coarse gain of 5. The dose rate we used were 0.1 mSv/h, 0.5 mSv/h, 0.75mSv/h and 1.0 mSv/h. In Figure 4.9 is shown microdosimetric distribution yd(y) *vs.* lineal energy y.

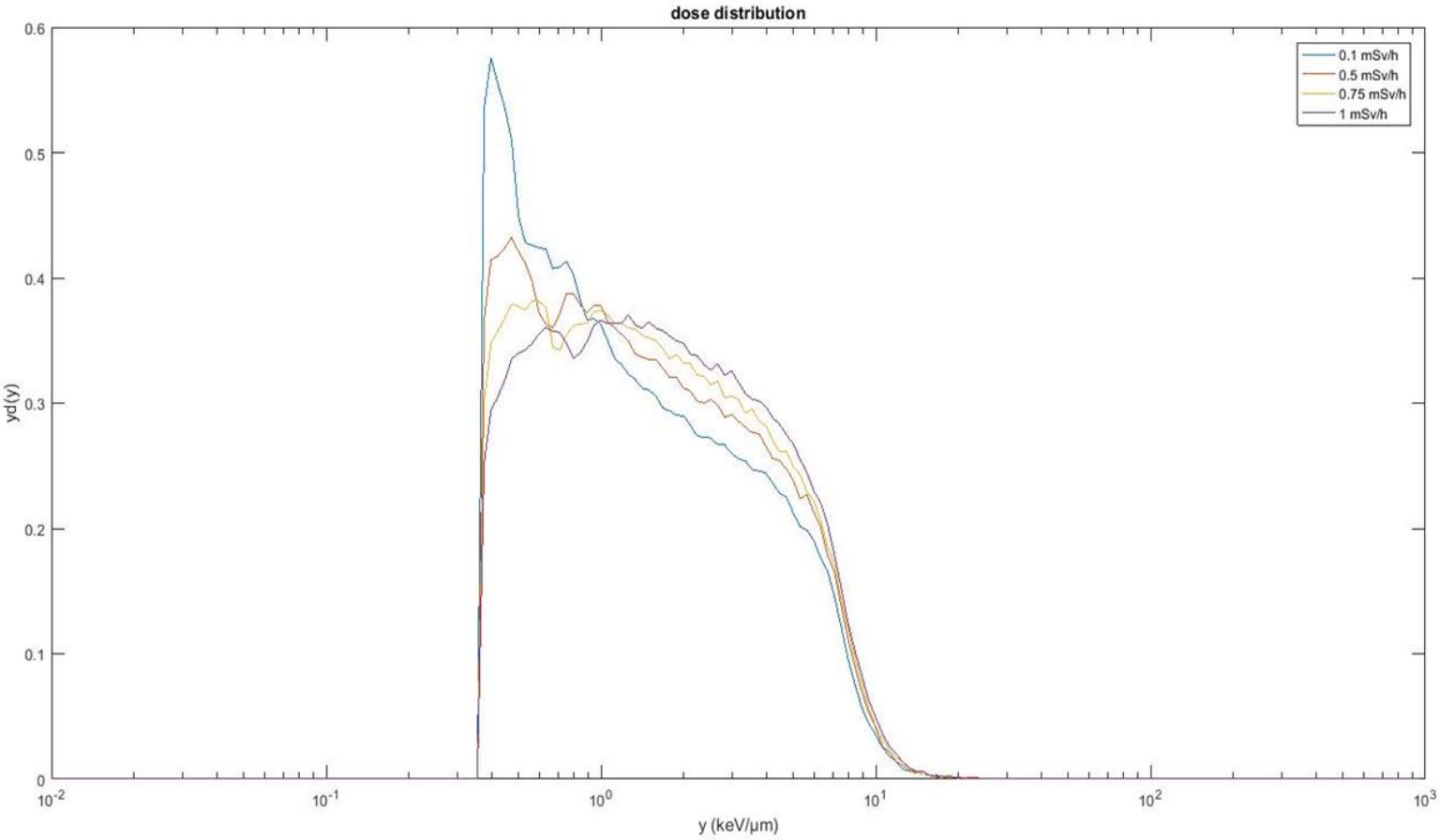

Figure 4.9 – Microdosimetric distribution yd(y) vs. y for ^{60}Co radiation at different dose rates.

In table 4.13 the settings used to take these measurements are shown.

Table 4.13 - Settings

Rise Time	4.8 µs
Flat Top	0.8 µs
BLR Mode	auto
Pole 0	666
Gain	5x
FDISC	Manual, 2.0%
LLD	Manual, 0.4%

The measurement performed in a gamma source (^{60}Co) is shown below. This measurement was taken with Ortec preamp and CAEN acquisition system with an applied voltage of 750V and a coarse gain of 1.0. In Figure 4.10 is shown microdosimetric distribution yd(y) *vs*. lineal energy y.

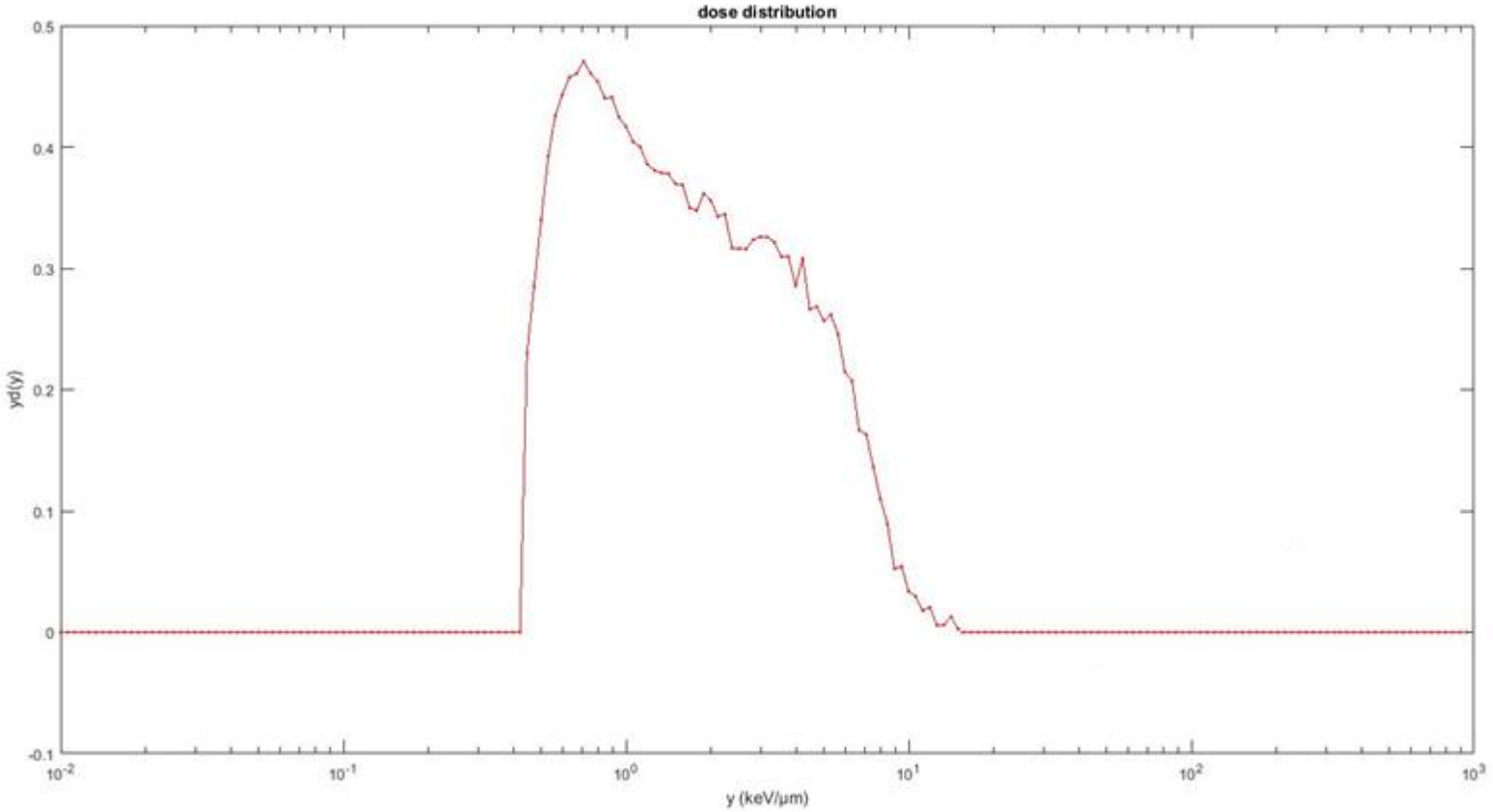

Figure 4.10 - Microdosimetric distribution yd(y) vs. y for ^{60}Co radiation.

In table 4.14 the settings used to take this measurement are shown.

Table 4.14 - Settings

Dynamic Range	3.7 Vpp
Decimator	8
Digital Gain	1
Input Rise Time	6.7 µs
Trigger Hold Off	5.04 µs
Threshold	30 LSB
Trapezoidal Rise Time	8.4 µs
Trapezoidal Decay Time	74.8 µs
Trapezoidal Flat Top	15.00 µs
Trapezoidal Gain	1

9.3. ^{252}Cf irradiations

The measurement performed in a neutron source (^{252}Cf) is shown below. This measurement was taken with Ortec preamp and CAEN acquisition system with applied voltage of 670V and a coarse gain of 1.0. In Figure 4.11 is shown microdosimetric distribution yd(y) *vs*. lineal energy.

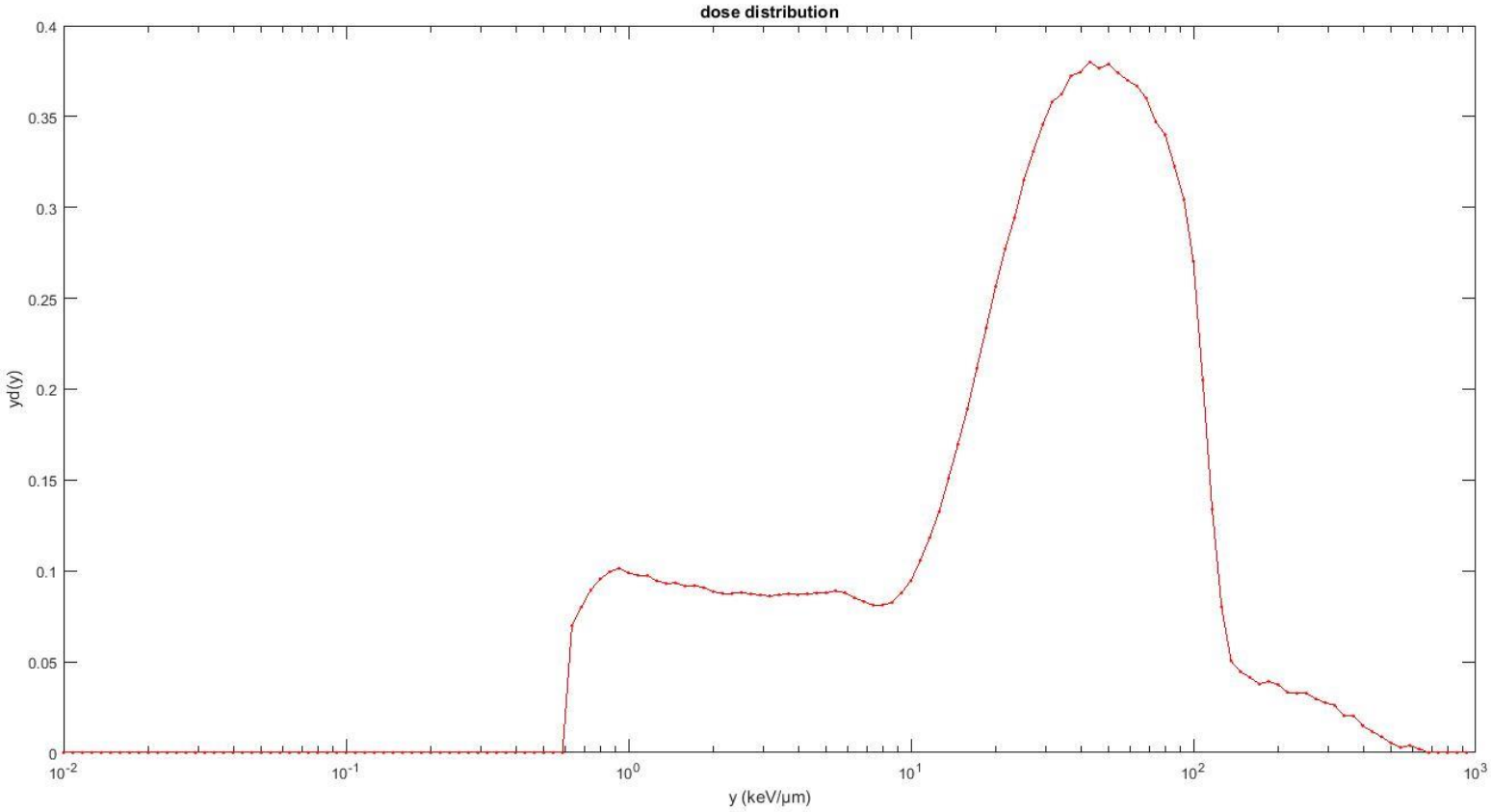

Figure 4.11 - Microdosimetric distribution yd(y) vs. y for ^{252}Cf radiation, measured with Ortec preamp and system acquisition CAEN with an applied voltage of 670V.

In table 4.15 the settings used to take this measurement are shown.

Table 4.15 - Settings

Dynamic Range	9.5 Vpp
Decimator	8
Digital Gain	1
Input Rise Time	6.7 µs
Trigger Hold Off	5.04 µs
Threshold	10 LSB
Trapezoidal Rise Time	8.4 µs
Trapezoidal Decay Time	74.8 µs
Trapezoidal Flat Top	15.00 µs
Trapezoidal Gain	1

The measurements performed in a neutron source (^{252}Cf) are shown below. This measurements were taken with SCK preamp and Inspector acquisition system with an applied voltage of 750V and a coarse gain of 2,5. The dose rate we used were 2 mSv/h, and 0.461 mSv/h.

In Figure 4.12 is shown a comparison between the microdosimetric distribution yd(y) *vs*. lineal energy y at the two different dose rates.

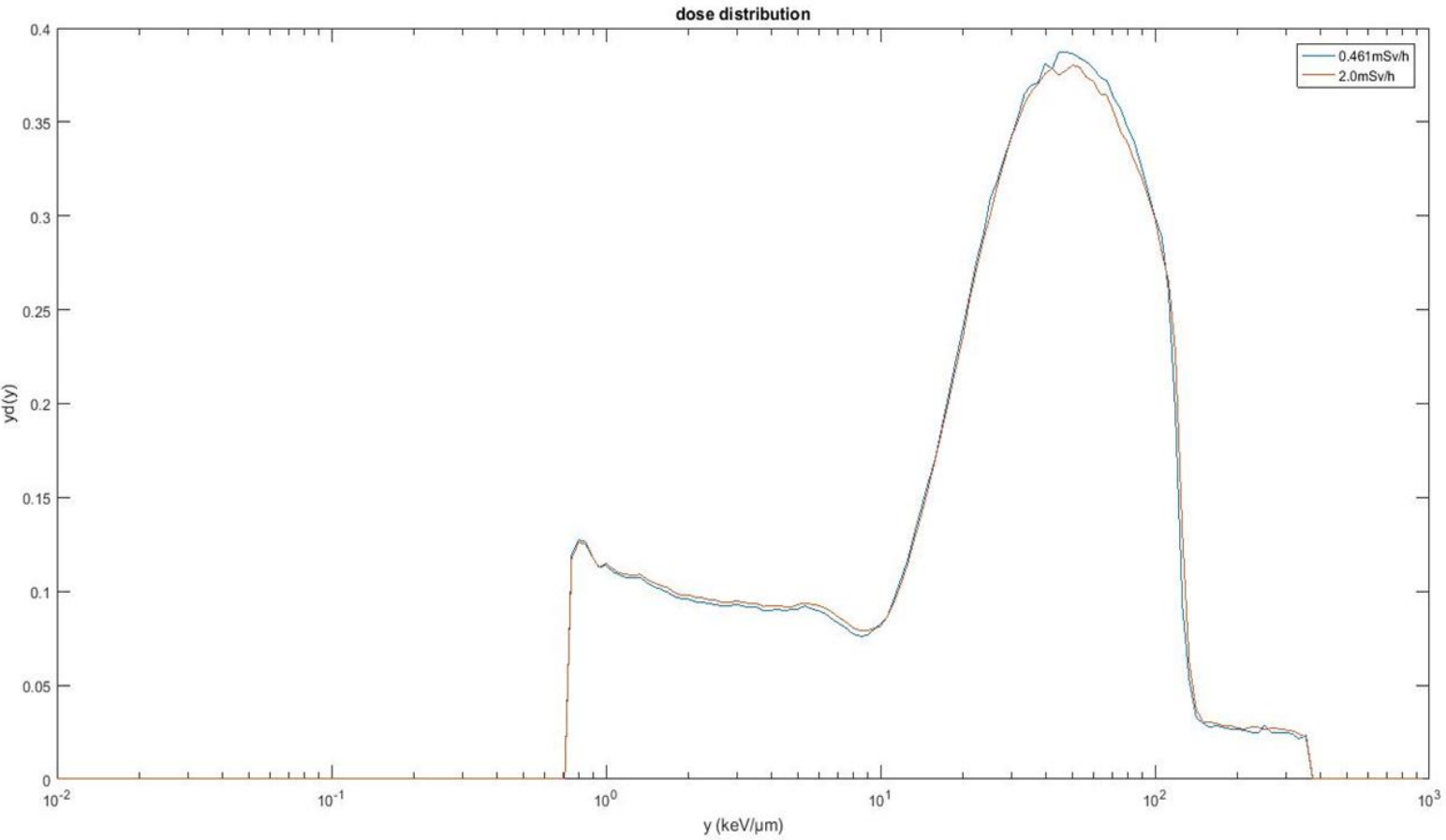

Figure 4.12 - Microdosimetric distribution yd(y) vs. y for ^{252}Cf radiation at different dose rates.

In table 4.16 the settings used to take these measurements are shown.

Table 4.16 - Settings

Rise Time	4.8 µs
Flat Top	0.8 µs
BLR Mode	auto
Pole 0	666
Gain	5x
FDISC	Manual, 2.0%
LLD	Manual, 0.6%

The measurement performed in a neutron source (^{252}Cf) is shown below. This measurement was taken with SCK preamp and CAEN acquisition system with an applied voltage of 700V and a coarse gain of 1.0.

In Figure 4.13 is shown microdosimetric distribution yd(y) *vs*. lineal energy y.

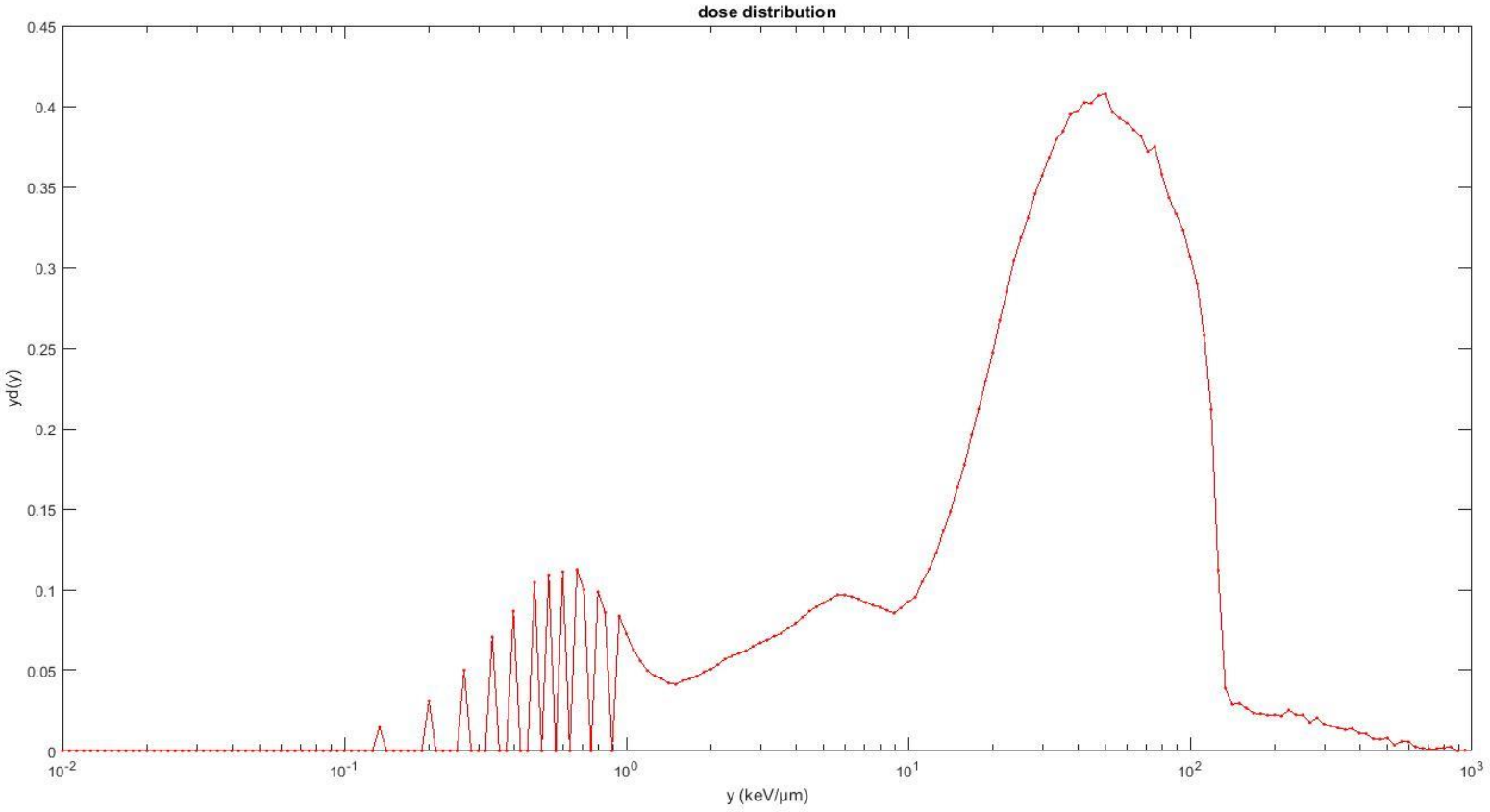

Figure 4.13 - Microdosimetric distribution yd(y) vs. y for ^{252}Cf radiation, measured with SCK preamp and CAEN acquisition system with an applied voltage of 700V.

In table 4.17 the settings used to take this measurement are shown.

Table 4.17 - Settings

Dynamic Range	9.5 Vpp
Decimator	8
Digital Gain	1
Input Rise Time	8.3 µs
Trigger Hold Off	5.04 µs
Threshold	45 LSB
Trapezoidal Rise Time	34 µs
Trapezoidal Decay Time	113 µs
Trapezoidal Flat Top	30.00 µs
Trapezoidal Gain	1

The measurement performed in a neutron source (^{252}Cf) is shown below. This measurement was taken with Ortec preamp and Inspector acquisition system with an applied voltage of 630V and a coarse gain of 2.5. In Figure 4.14 is shown microdosimetric distribution yd(y) *vs*. lineal energy y.

In table 4.18 the settings used to take this measurement are shown.

Table 4.18 - Settings

Rise Time	4.8 µs
Flat Top	1.0 µs
BLR Mode	Medium
Pole 0	666
Gain	2.5x
FDISC	Manual, 3.0%
LLD	Manual, 0.2%

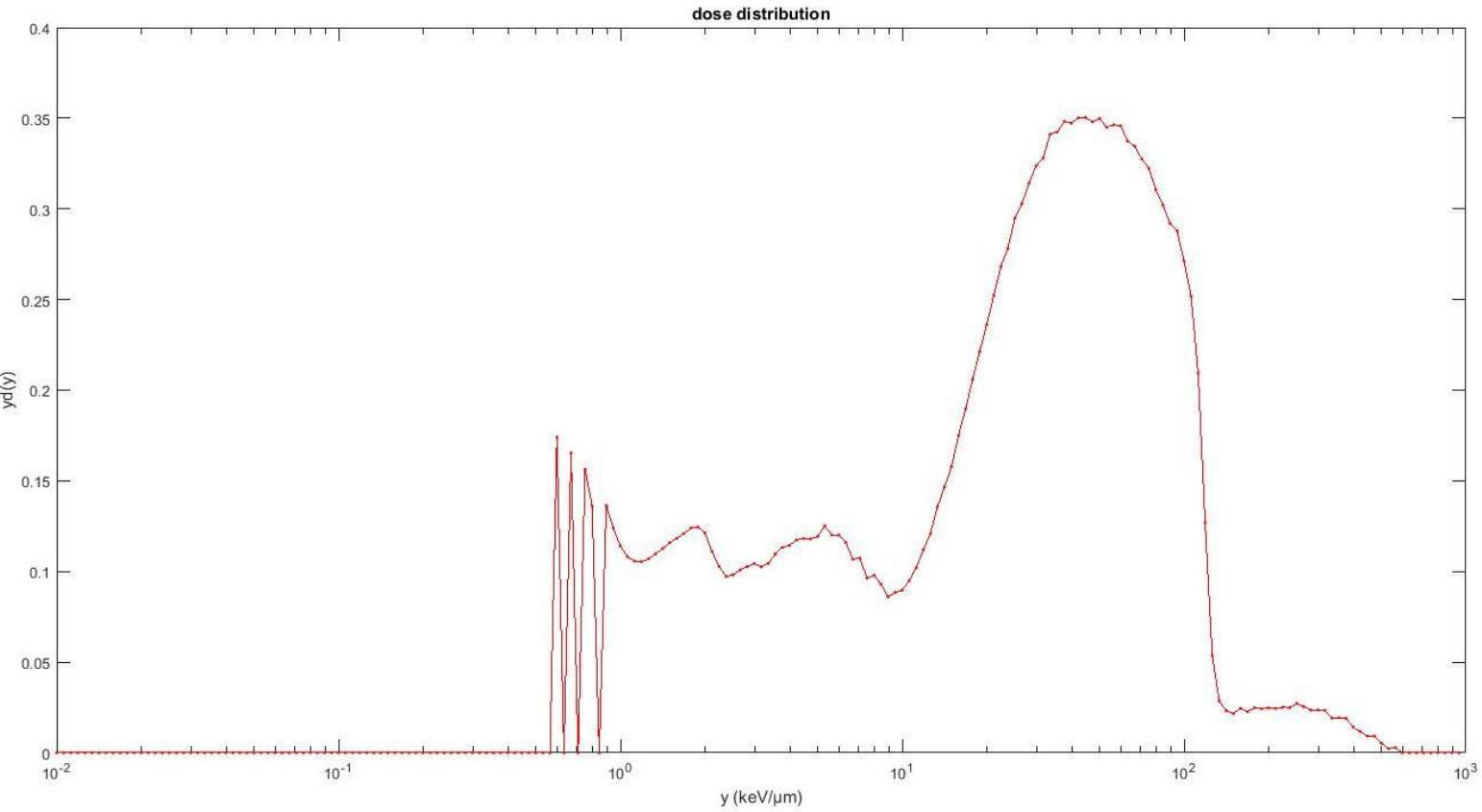

Figure 4.14 - Microdosimetric distribution yd(y) vs. y for ^{252}Cf radiation, measured with Ortec pramp and system acquisition Inspector with an applied voltage of 630V.

The measurement performed in a neutron source (^{252}Cf) is shown below. This measurement was taken with Ortec preamp and CAEN acquisition system with an applied voltage of 700V and a coarse gain of 1.0. In Figure 4.15 is shown microdosimetric distribution yd(y) *vs*. lineal energy y.

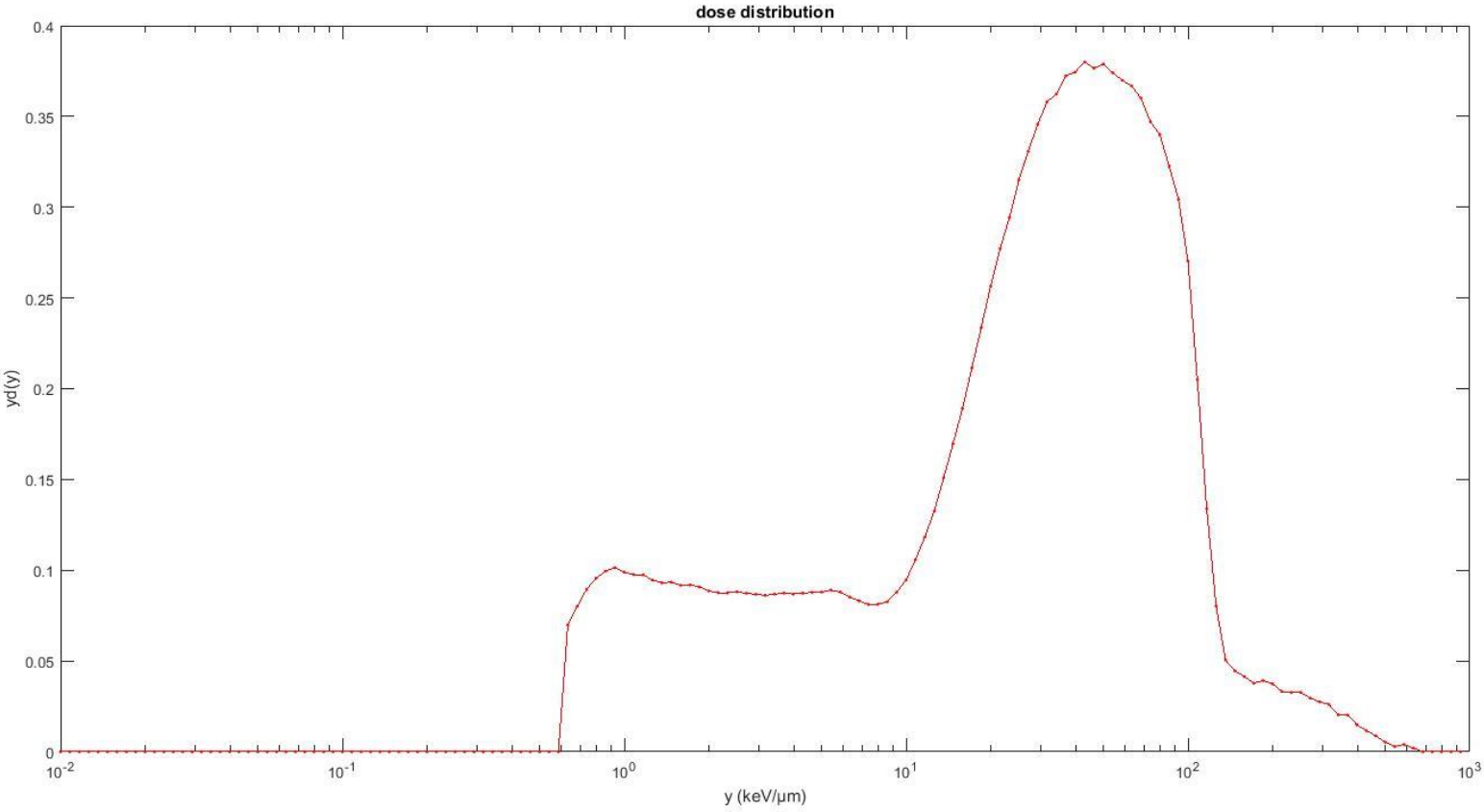

Figure 4.15 - Microdosimetric distribution yd(y) vs. y for ^{252}Cf radiation, measured with Ortec pramp and system acquisition CAEN with an applied voltage of 700V.

In table 4.19 the settings used to take this measurement are shown.

Table 4.19 - Settings

Dynamic Range	9.5 Vpp
Decimator	8
Digital Gain	1
Input Rise Time	6.7 µs
Trigger Hold Off	5.04 µs
Threshold	14 LSB
Trapezoidal Rise Time	8.4 µs
Trapezoidal Decay Time	74.8 µs
Trapezoidal Flat Top	15.00 µs
Trapezoidal Gain	1

The measurement performed in a neutron source (^{252}Cf) is shown below. This measurement was taken with SCK preamp and Inspector acquisition system with an applied voltage of 670 V and a coarse gain of 2.5. In Figure 4.16 is shown microdosimetric distribution yd(y) *vs.* lineal energy y.

In table 4.20 the settings used to take this measurement are shown.

Table 4.20 - Settings

Rise Time	4.8 µs
Flat Top	1.0 µs
BLR Mode	Medium
Pole 0	666
Gain	2.5x
FDISC	Manual, 3.0%
LLD	Manual, 0.2%

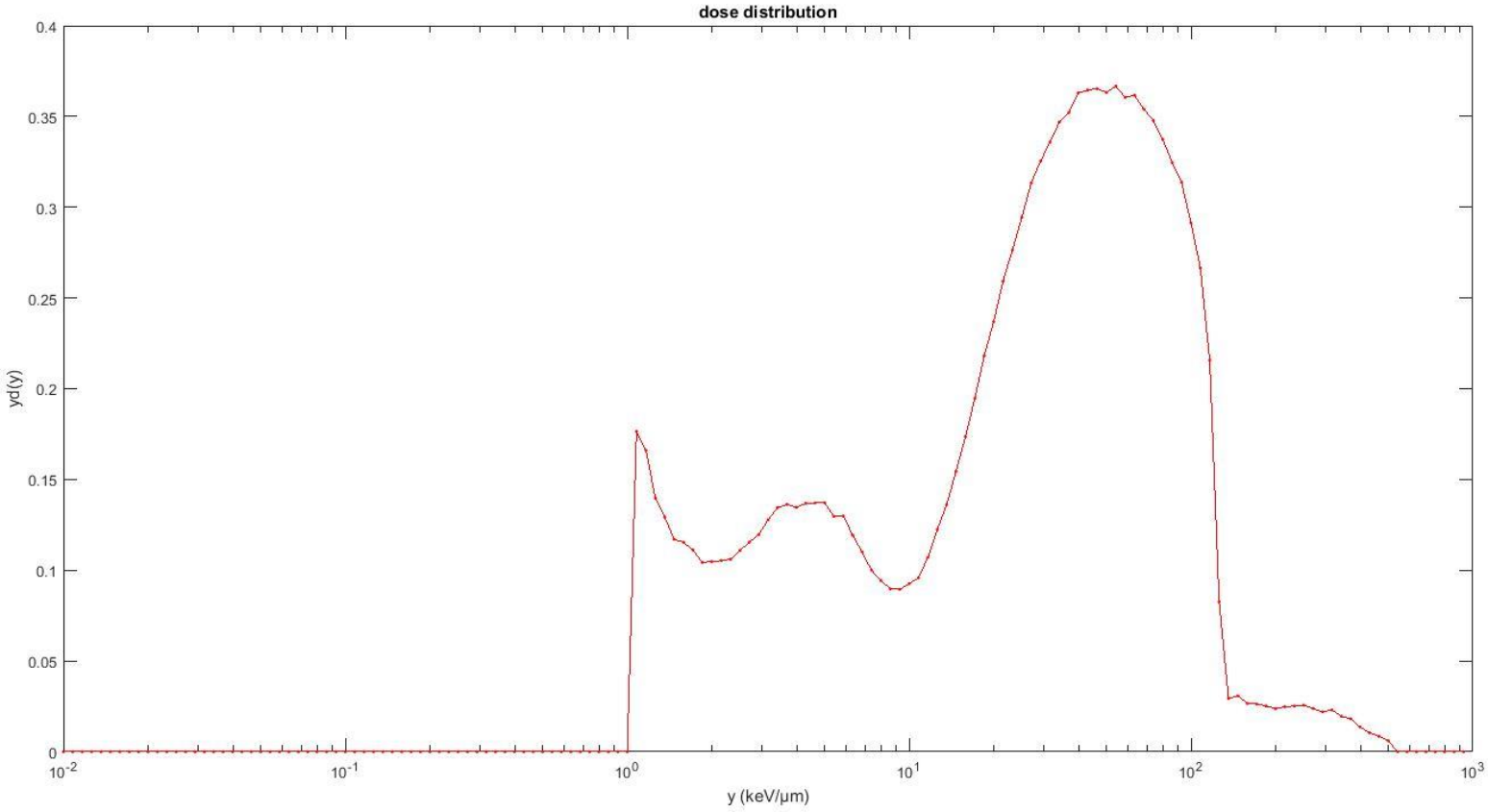

Figure 4.16 - Microdosimetric distribution yd(y) vs. y for ^{252}Cf radiation, measured with SCK pramp and Inspector acquisition system with an applied voltage of 670V.

9.4. BR1 Channel z55 measurements

The measurements performed in a mixed gamma-neutron field at z55 channel of the SCK reactor BR1 are shown below. These measurements were taken with Ortec preamp and CAEN acquisition system with applied voltages of 600V, 630V, 650V, 700V and a coarse gain of 1.0.

In Figure 4.17 are shown microdosimetric distributions yd(y) *vs.* lineal energy y for the 4 measurements at different voltages.

In Figure 4.18 are shown microdosimetric distributions yd(y) *vs.* lineal energy y for the 4 measurements at different voltages, cut at *4.1 [keV/ µm].*

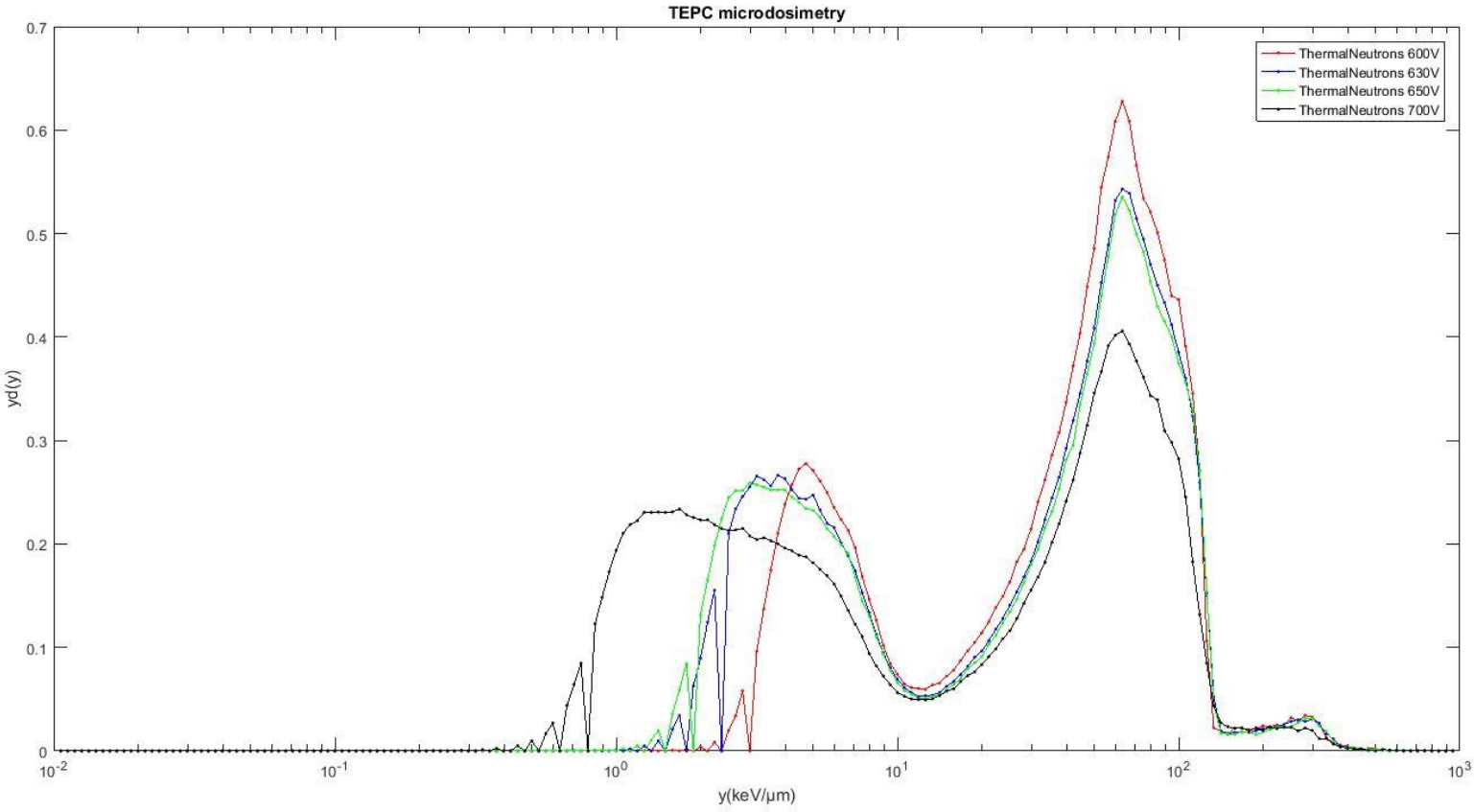

Figure 4.17 - Comparison between the microdosimetric distribution yd(y) vs lineal energy y measurements obtained at different voltages in a mixed gamma-neutron field at z55 channel of the SCK reactor BR1.

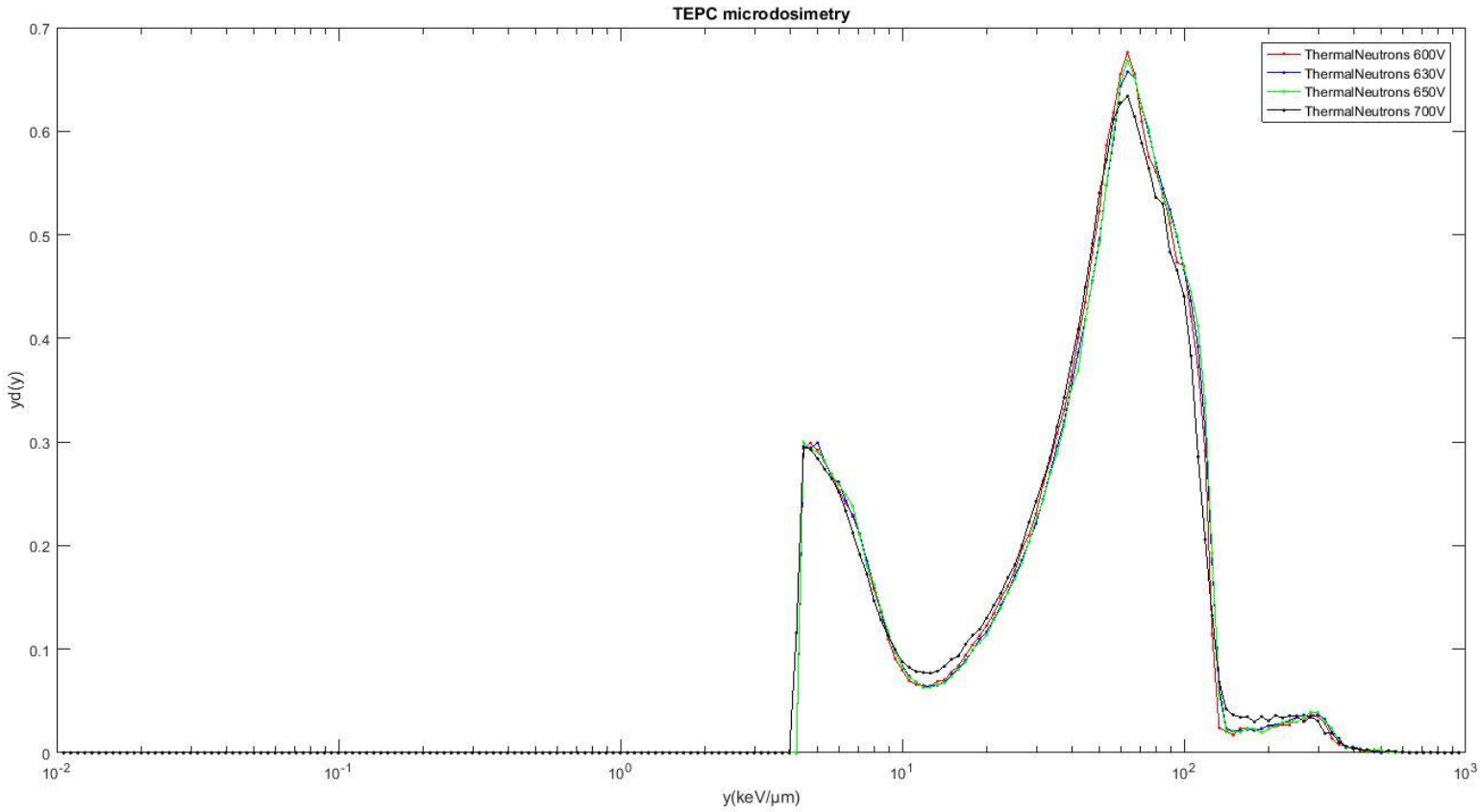

Figure 4.18 - Comparison between the microdosimetric distribution yd(y) vs lineal energy y measurements obtained at different voltages in a mixed gamma-neutron field at z55 channel of the SCK reactor BR1, cut at 4.1 [keV/ µm].

In table 4.21 the settings used to take these measurements are shown.

Table 4.21 - Settings

Dynamic Range	9.5 Vpp
Decimator	8
Digital Gain	1
Input Rise Time	6.7 µs
Trigger Hold Off	5.04 µs
Threshold	14 LSB
Trapezoidal Rise Time	8.4 µs
Trapezoidal Decay Time	74.8 µs
Trapezoidal Flat Top	15.00 µs
Trapezoidal Gain	1

The measurements performed in a mixed gamma-neutron field at z55 channel of the SCK reactor BR1 are shown below. These measurements were taken with Ortec preamp and Inspector acquisition system with applied voltages of 600V, 630V, 650V, 670V and a coarse gain of 2.5.

In table 4.21 the settings used to take these measurements are shown.

Table 4.22 - Settings

Rise Time	4.8 µs
Flat Top	1.0 µs
BLR Mode	Medium
Pole 0	666
Gain	2.5x
FDISC	Manual, 3.0%
LLD	Manual, 0.2%

In Figure 4.19 are shown microdosimetric distributions yd(y) *vs*. lineal energy y for the 4 measurements at different voltages.

In Figure 4.20 are shown microdosimetric distributions yd(y) *vs*. lineal energy y for all the measurements obtained in BR1at different voltages, cut at *4.1 [keV/ µm].*

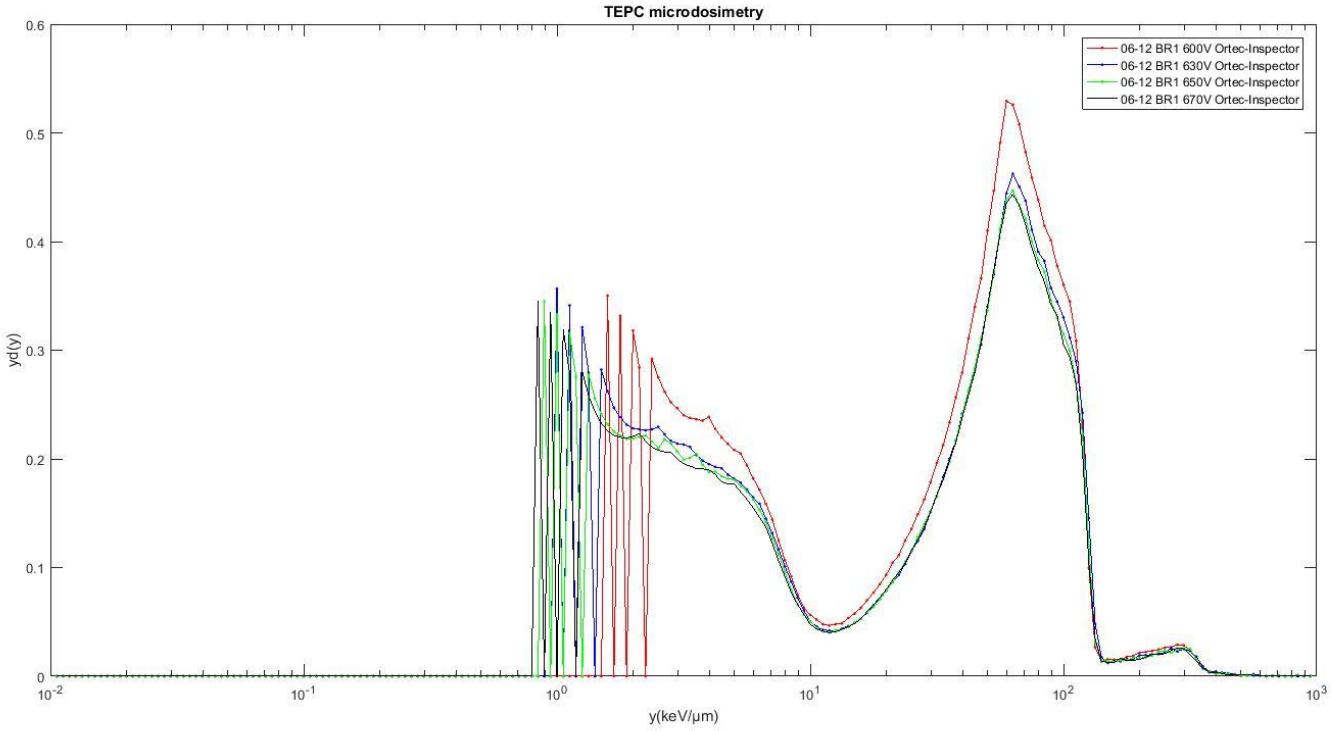

Figure 4.19 - Comparison between the microdosimetric distribution yd(y) vs lineal energy y measurements obtained at different voltages in a mixed gamma-neutron field at z55 channel of the SCK reactor BR1.

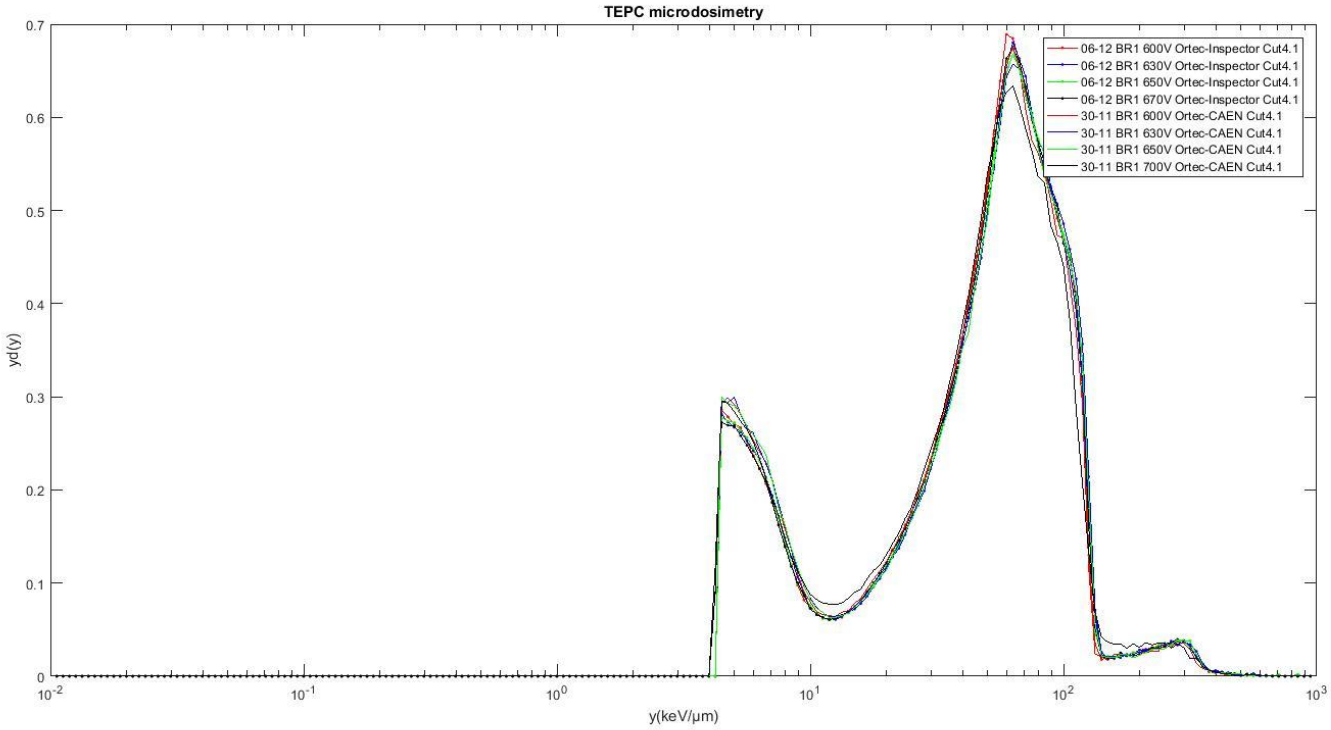

Figure 4.20 - Comparison between the microdosimetric distribution yd(y) vs lineal energy y measurements obtained at different voltages in a mixed gamma-neutron field at z55 channel of the SCK reactor BR1 with both InSpector and CAEN acquisition system.

Chap. 10. Spectra analysis and microdosimetric quantity tables

In figure 5.1 a comparison between the microdosimetric distribution yd(y) *vs*. lineal energy y measurements taken in ^{252}Cf source is shown.

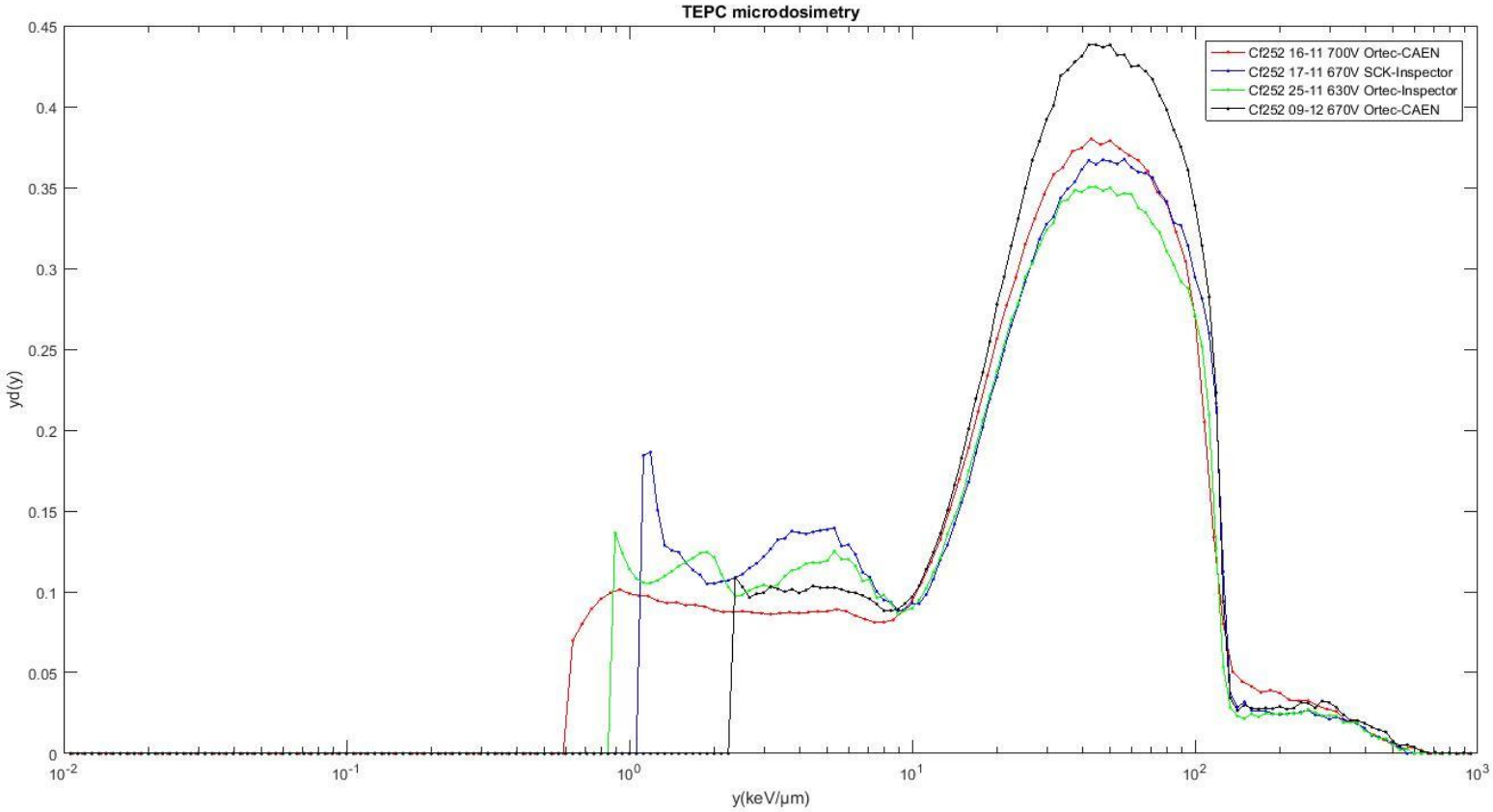

Figure 5.1 - Comparison between the microdosimetric distribution yd(y) vs lineal energy y measurements in ^{252}Cf source from 16/11 (Ortec-CAEN Setup), 17/11 (SCK-Inspector Setup) 25/11 (Ortec-Inspector Setup) and 09/12 (Ortec-CAEN setup).

In figure 5.1 are visible the problems we have if we do not put the high voltage filters (green and blue lines) or if we put too high voltage to the TEPC (red line).

In figure 5.2 a reference spectra for ^{252}Cf is shown.[15]

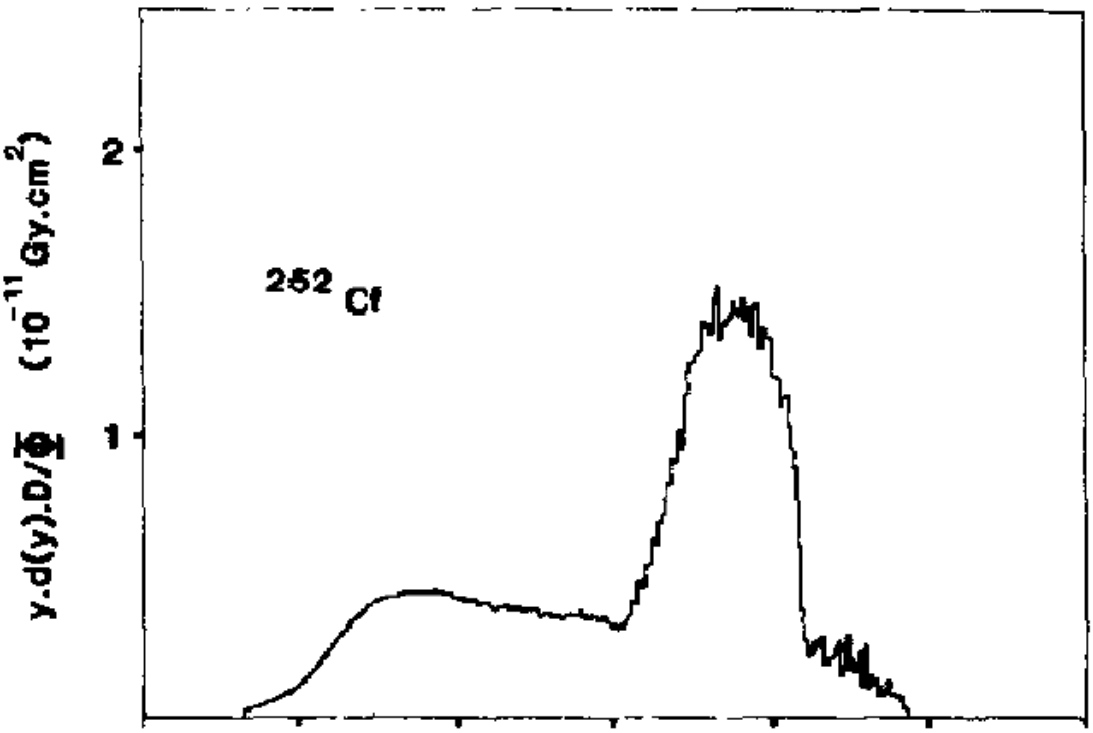

Figure 5.2 - reference spectra for ^{252}Cf.[15]

In table 5.1 the most significant dosimetric and microdosimetric values obtained from the measurements in the neutron source ^{252}Cf are shown.

Table 5.1 - Most significant dosimetric and microdosimetric values obtained from the measurements in the neutron source ^{252}Cf.

TEPC analysis					
Reference values	**Spectra Source**	^{252}Cf	^{252}Cf	^{252}Cf	^{252}Cf
	Date	2016-11-16	2016-11-17	2016-11-25	2016-12-09
	H*(10) [µSv/h]	410.26	409.97	407.62	402.76
TEPC settings	**Preamplifier**	Ortec	SCK	Ortec	Ortec
	Acquisition system	CAEN	Inspector	Inspector	CAEN
	Gain	gain 1.0	gain 2.5	gain 2,5	gain 1.0
	Voltage [V]	700	670	630	670
Measured values from the spectra	**Absorbed dose rate D (µGy/h)**	39.92	42.99	41.42	36.39
	$\sigma_{D/t}$ (µGy/h)	0.03640	0.03796	0.03513	0.04646
	Q [Sv/Gy]	9.85	10.19	9.60	11.51
	σ_Q [Sv/Gy]	0.008989	0.008999	0.008146	0.01469
	σ_Q/Q (%)	0.0912	0.0883	0.0848	0.1277
	Dose equivalent rate H [µSv/h]	393.27	438.32	397.84	418.97
	σ_H [µSv/h]	0.5075	0.5472	0.4772	0.7564
	Tot counts	8719577	6690433	8466904	1806304
Microdosimetric quantities - Measured values from the spectra	**$\overline{y_F}$ [keV/um]**	5.89	8.27	6.71	16.85
	σ_{yF} [keV/um]	0.0054	0.0073	0.0057	0.0215
	σ_{yF}/yf (%)	0.0912	0.0883	0.0848	0.1277
	$\overline{y_D}$ [keV/um]	42.77	43.12	40.90	49.62
	σ_{yD} [keV/um]	0.1354	0.1230	0.1208	0.1973
	σ_{yD}/yD (%)	0.3166	0.2851	0.2955	0.3977
	R_H=H /H*(10)	1.04	0.93	1.02	0.96

In figure 5.3 a comparison between the microdosimetric distribution yd(y) vs lineal energy y measurements taken in z55 channel of reactor BR1 in data 30/11 is shown. The acquisition configuration is preamp Ortec-acquisition system CAEN.

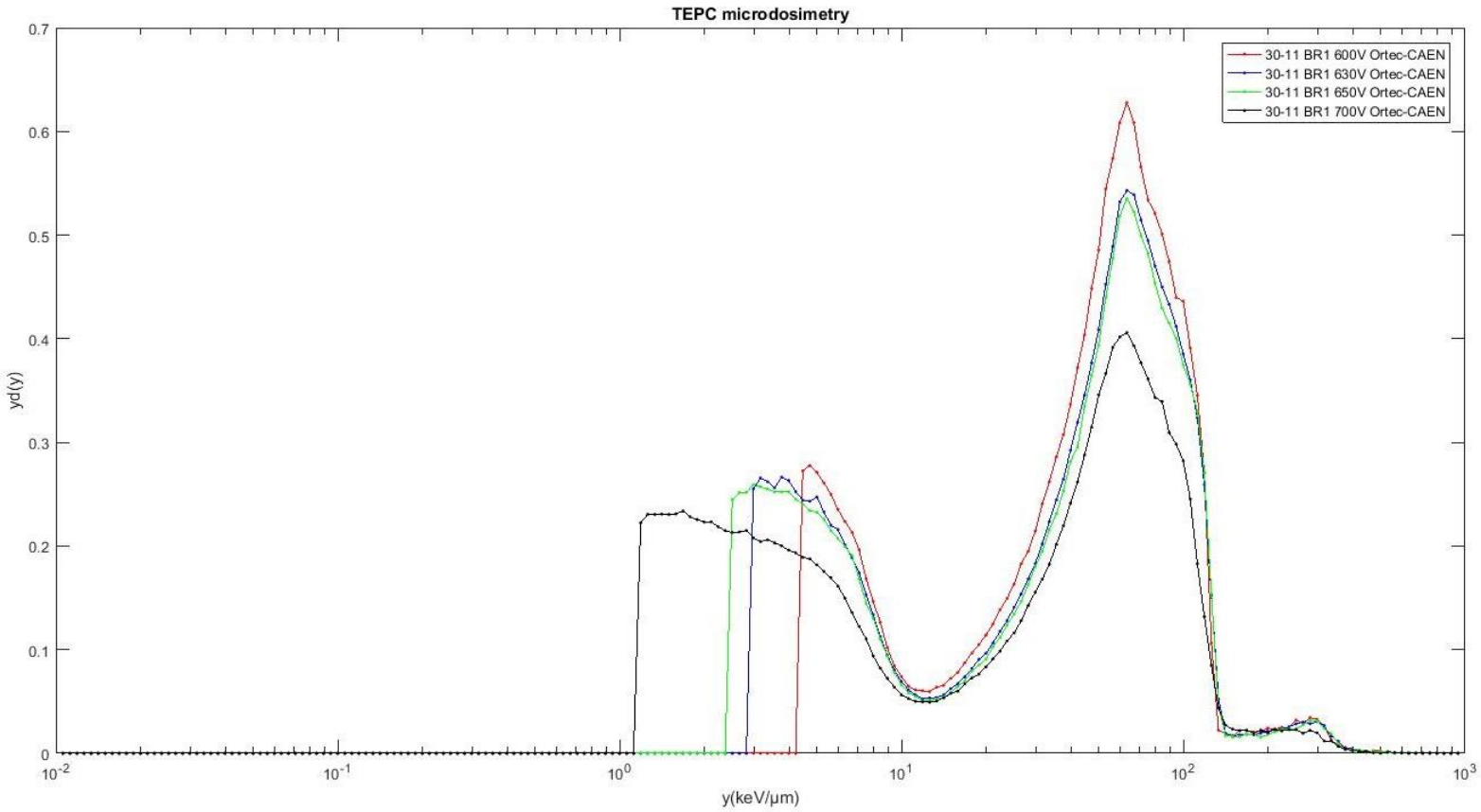

Figure 5.3 - Comparison between the microdosimetric distribution yd(y) vs lineal energy y measurements taken in z55 channel of reactor BR1 in data 30/11.

In table 5.2 the most significant dosimetric and microdosimetric values obtained from the measurements in z55 channel in BR1in data 30/11 are shown.

Table 5.2 - Most significant dosimetric and microdosimetric values obtained from the measurements in z55 channel in BR1 (Ortec-CAEN).

TEPC analysis					
Reference values	**Spectra Source**	z55 BR1	z55 BR1	z55 BR1	z55 BR1
	Date	2016-11-30	2016-11-30	2016-11-30	2016-11-30
	H*(10) [µSv/h]	3485.91	3485.91	3485.91	3485.91
TEPC settings	**Preamplifier**	Ortec	Ortec	Ortec	Ortec
	Acquisition system	Caen	Caen	Caen	Caen
	Gain	gain 1,0	gain 1,0	gain 1,0	gain 1,0
	Voltage [V]	600	630	650	700
Measured values from the spectra	**Absorbed dose rate D (µGy/h)**	255.36	252.27	268.30	251.00
	$\sigma_{D/t}$ (µGy/h)	0.40369	0.28705	0.43315	0.33606
	Q [Sv/Gy]	13.54	13.75	13.80	13.21
	σ_Q [Sv/Gy]	0.021402	0.015647	0.022281	0.017683
	σ_Q/Q (%)	0.1581	0.1138	0.1614	0.1339
	Dose equivalent rate H [µSv/h]	3456.90	3469.00	3702.77	3314.99
	σ_H [µSv/h]	7.7287	5.5822	8.4541	6.2769
	Tot counts	1063583	2100137	1044581	1506633
Microdosimetric quantities - Measured values from the spectra	**$\overline{y_F}$ [keV/um]**	20.23	20.26	20.27	19.67
	σ_{yF} [keV/um]	0.0320	0.0230	0.0327	0.0263
	σ_{yF}/yf (%)	0.1581	0.1138	0.1614	0.1339
	$\overline{y_D}$ [keV/um]	53.76	55.09	55.19	53.12
	σ_{yD} [keV/um]	0.1857	0.1378	0.1933	0.1569
	σ_{yD}/yD (%)	0.3454	0.2502	0.3503	0.2954
	R_H=H /H*(10)	1.01	1.00	0.94	1.05

In figure 5.4 a comparison between the microdosimetric distribution yd(y) vs lineal energy y measurements taken in z55 channel of reactor BR1 in data 06/12 is shown. The acquisition configuration is preamp Ortec-acquisition system Inspector.

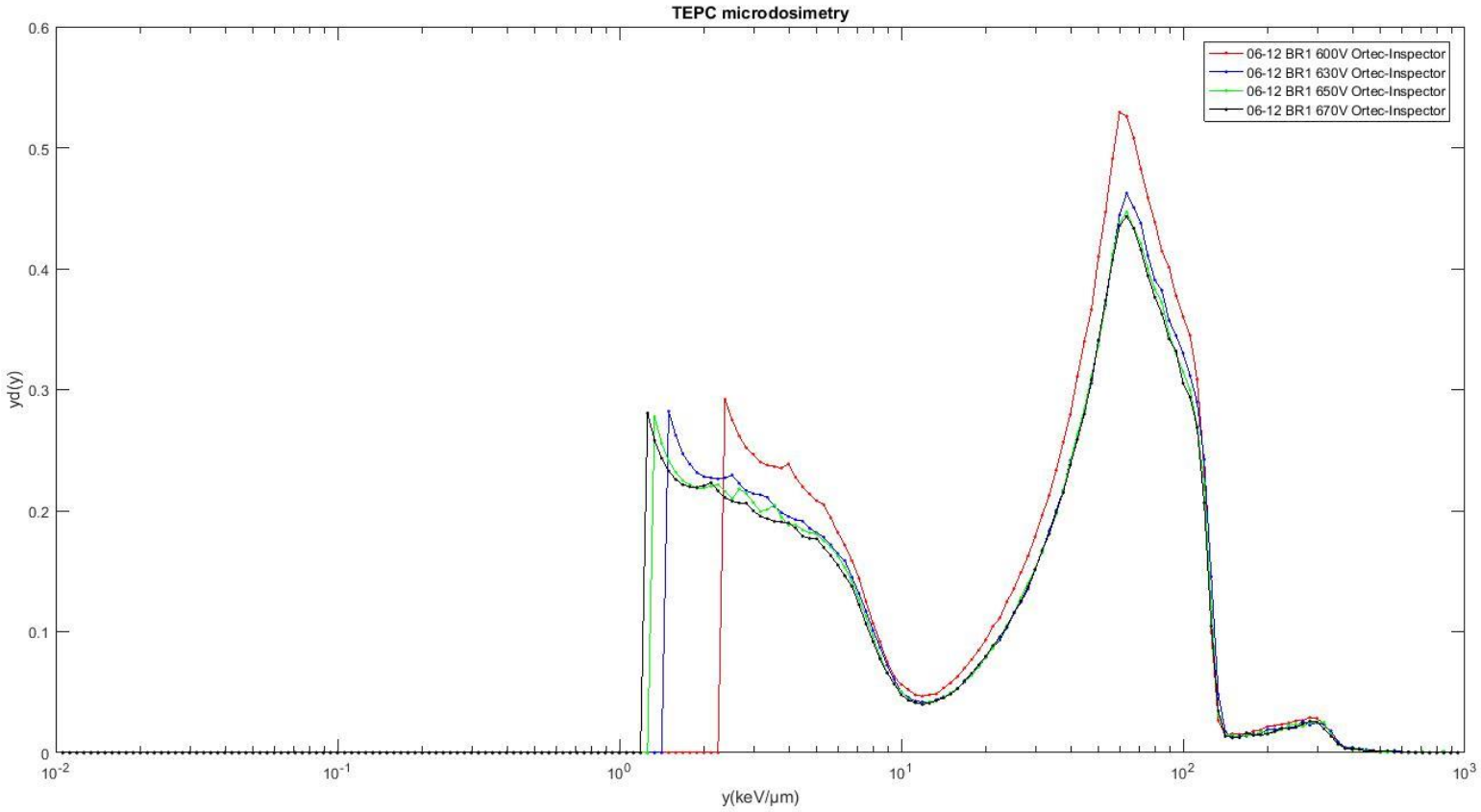

Figure 5.4 - Comparison between the microdosimetric distribution yd(y) vs lineal energy y measurements taken in z55 channel of reactor BR1 in data 30/1.

In table 5.3 the most significant dosimetric and microdosimetric value obtained from the measurements in z55 channel in BR1 in data 06/12 are shown.

Table 5.3 - Most significant dosimetric and microdosimetric value obtained from the measurements in z55 channel in BR1 (Ortec-Inspector).

TEPC analysis					
Reference values	**Spectra Source**	z55 BR1	z55 BR1	z55 BR1	z55 BR1
	Date	2016-12-06	2016-12-06	2016-12-06	2016-12-06
	H*(10) [µSv/h]	4713.80	4713.80	4713.80	4713.80
TEPC settings	**Preamplifier**	Ortec	Ortec	Ortec	Ortec
	Acquisition system	Inspector	Inspector	Inspector	Inspector
	Gain	gain 2,5	gain 2,5	gain 2,5	gain 2,5
	Voltage [V]	600	630	650	670
Measured values from the spectra	**Absorbed dose rate D (µGy/h)**	426.44	472.20	485.89	512.14
	$\sigma_{D/t}$ (µGy/h)	0.39323	0.45259	0.45312	0.36799
	Q [Sv/Gy]	10.89	9.92	9.61	9.48
	σ_Q [Sv/Gy]	0.010045	0.009505	0.008967	0.006812
	σ_Q/Q (%)	0.0922	0.0958	0.0933	0.0718
	Dose equivalent rate H [µSv/h]	4645.39	4682.67	4671.93	4855.20
	σ_H [µSv/h]	6.0579	6.3472	6.1615	4.9336
	Tot counts	6625685	8855410	10000580	17530510
Microdosimetric quantities - Measured values from the spectra	**$\overline{y_F}$ [keV/um]**	7.65	4.82	4.36	4.11
	σ_{yF} [keV/um]	0.0070	0.0046	0.0041	0.0029
	σ_{yF}/yf (%)	0.0922	0.0958	0.0933	0.0719
	$\overline{y_D}$ [keV/um]	43.08	39.20	37.90	37.18
	σ_{yD} [keV/um]	0.1076	0.1158	0.1162	0.0853
	σ_{yD}/yD (%)	0.2497	0.2954	0.3067	0.2295
	R_H=H /H*(10)	1.01	1.01	1.01	0.97

In figure 5.5 a reference spectra for thermal neutrons is shown.[14]

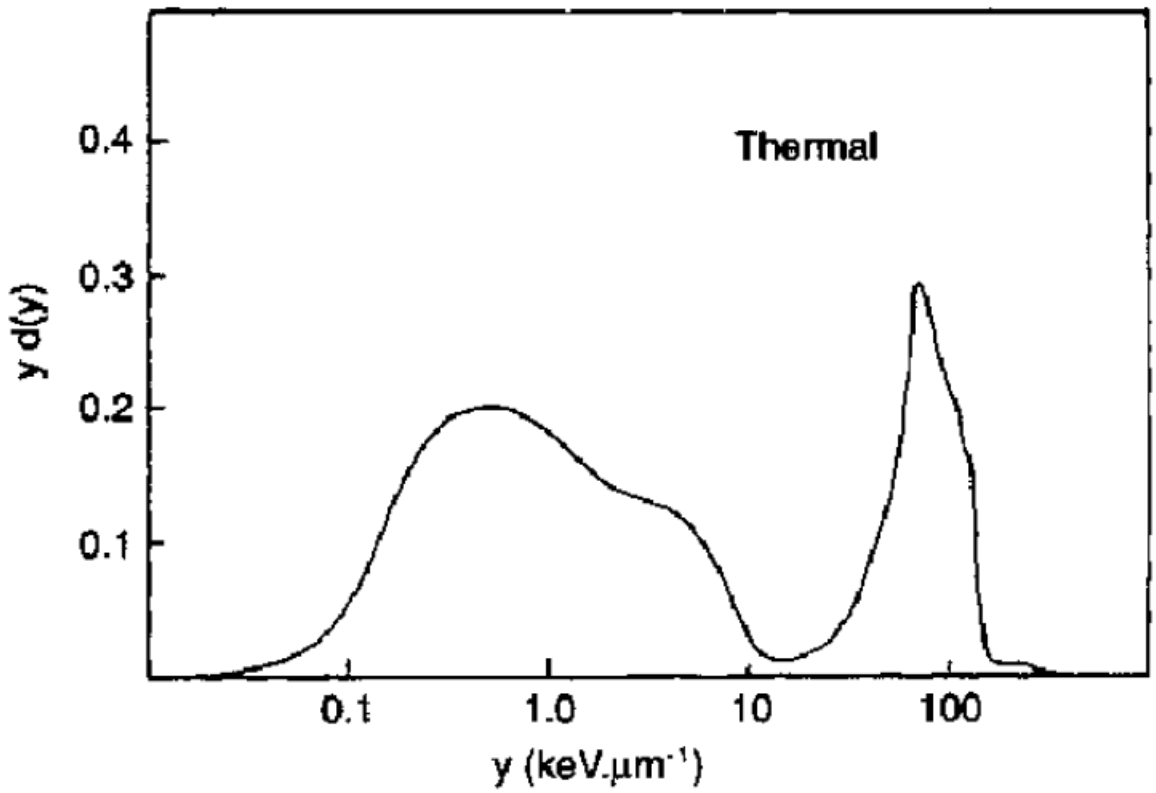

Figure 5.5 - Reference spectra for thermal neutrons.[14]

CONCLUSIONS

The aim of this thesis was to find the optimal measurement chain for a TEPC to be used in microdosimetry.

In this thesis we performed a systematic investigation measuring with a TEPC in different radiation fields to check the response of the new digital acquisition system (CAEN) to the variation of some parameters (Dose rate, type of radiation field, voltage applied to the TEPC, …) .

The ultimate goal of this work was to demonstrate the possibility to use the new acquisition system (CAEN) in an equivalent or better way than the one previously used (Inspector 2000). To do so, once we have been able to use the CAEN acquisition system to record the spectra of various sources with a good reliability, the final test was to measure the spectra with both the systems in a difficult to be replicated measurement situation (the z55 channel in BR1).

The goals achieved during this work are the following:

a) Through the acquisition chain optimization and playing with different settings we obtained stability and reproducibility. The electronic chain is now optimized for 4 different setups of Charge Sensitive Preamplifier and Acquisition System:

   - Ortec preamplifier – CAEN acquisition system
   - SCK preamplifier – Inspector acquisition system
   - Ortec preamplifier – Inspector acquisition system
   - Canberra preamplifier – CAEN acquisition system

   The first two listed configurations turned out to have the best features for our purpose, so these were the configurations chosen during the two days of testing we had available at BR1.

b) We verified the maximum voltage we can apply to the TEPC without losing linearity, immediately after the refilling it resulted to be 670 V. At the same time, we evaluated the various parameters that the software allows us to manipulate and we found the settings to have the best results with the CAEN acquisition system.

c) We performed microdosimetric measurements with the TEPC in gamma (^{137}Cs, ^{60}Co) and mixed gamma-neutron fields (^{252}Cf, BR1) and we obtained results with the CAEN acquisition system which are consistent with Inspector acquisition system.

d) We evaluated the main advantages that we will have using CAEN instead of Inspector and they have been listed out here:

- We exactly know what happens to the signal in every step of the acquisition chain.
- The possibility to change settings and to optimize for high resolution modality or high dose rate modality.
- The possibility to use simultaneously two channels and to set on them two different Dynamic Range.

APPENDIX A – PREAMPLIFIER SCHEMES

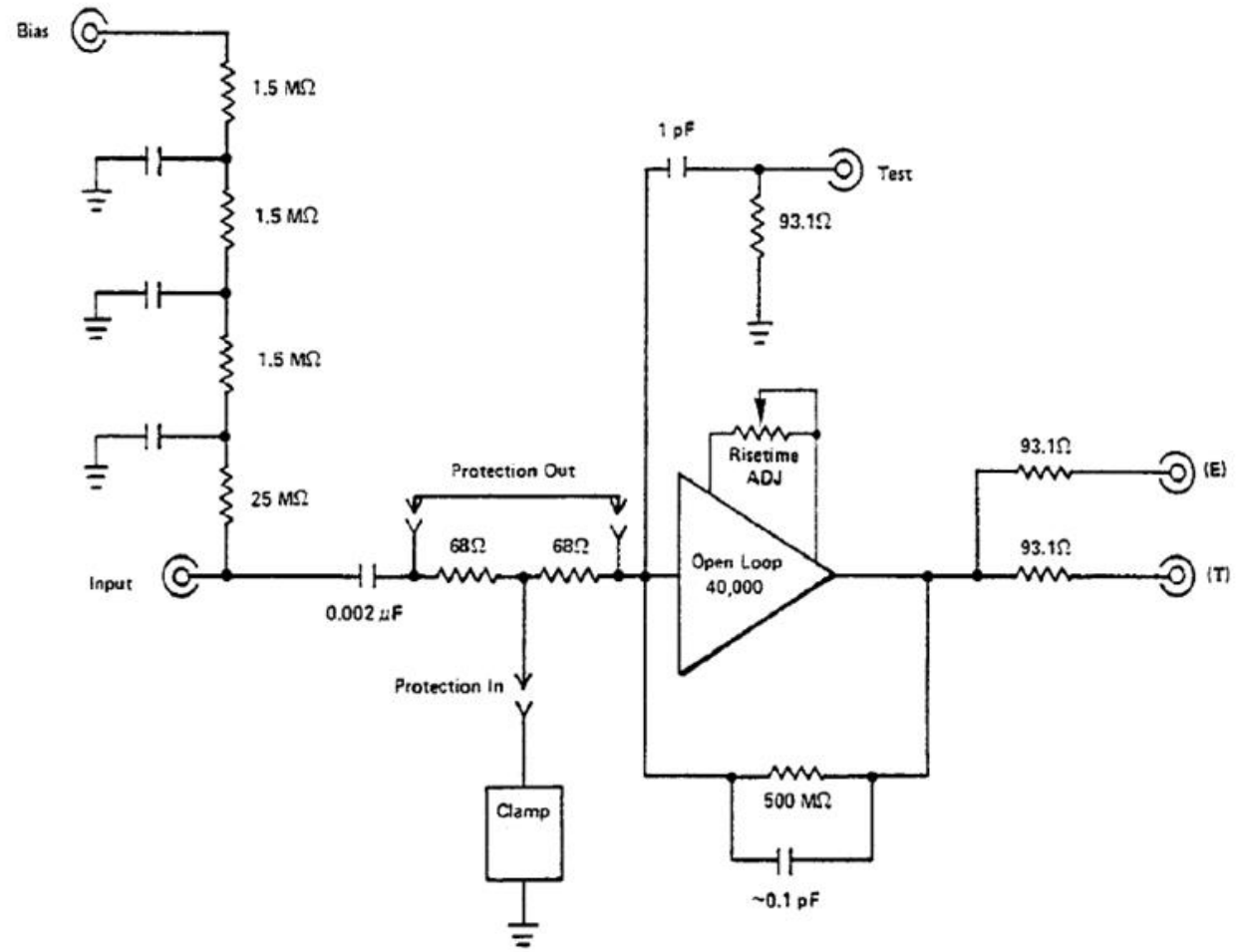

Figure A.1 – Scheme of the Ortec preamplifier. [22]

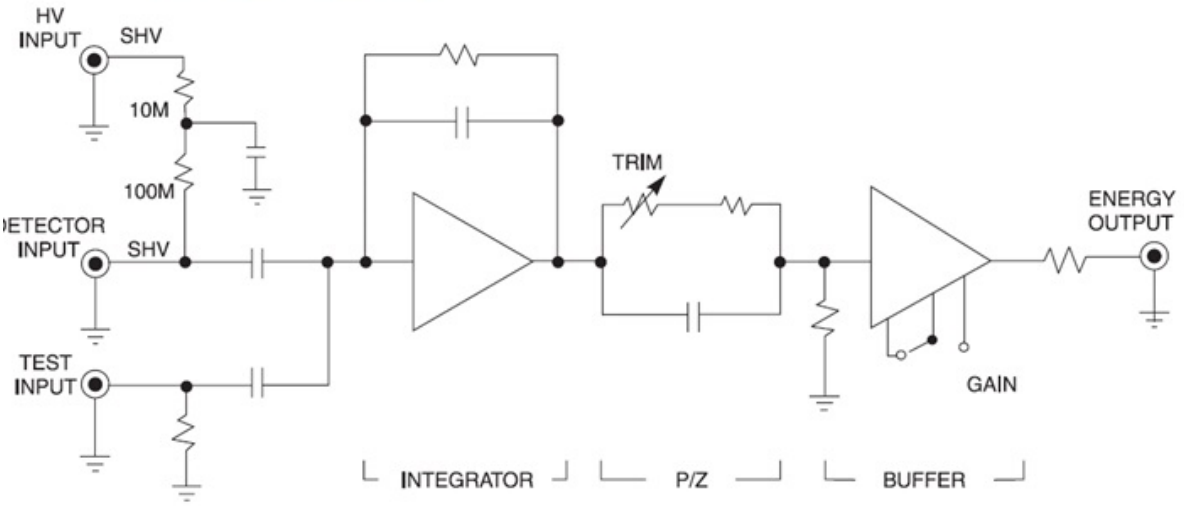

Figure A.2 – Scheme of the Canberra preamplifier. [21]

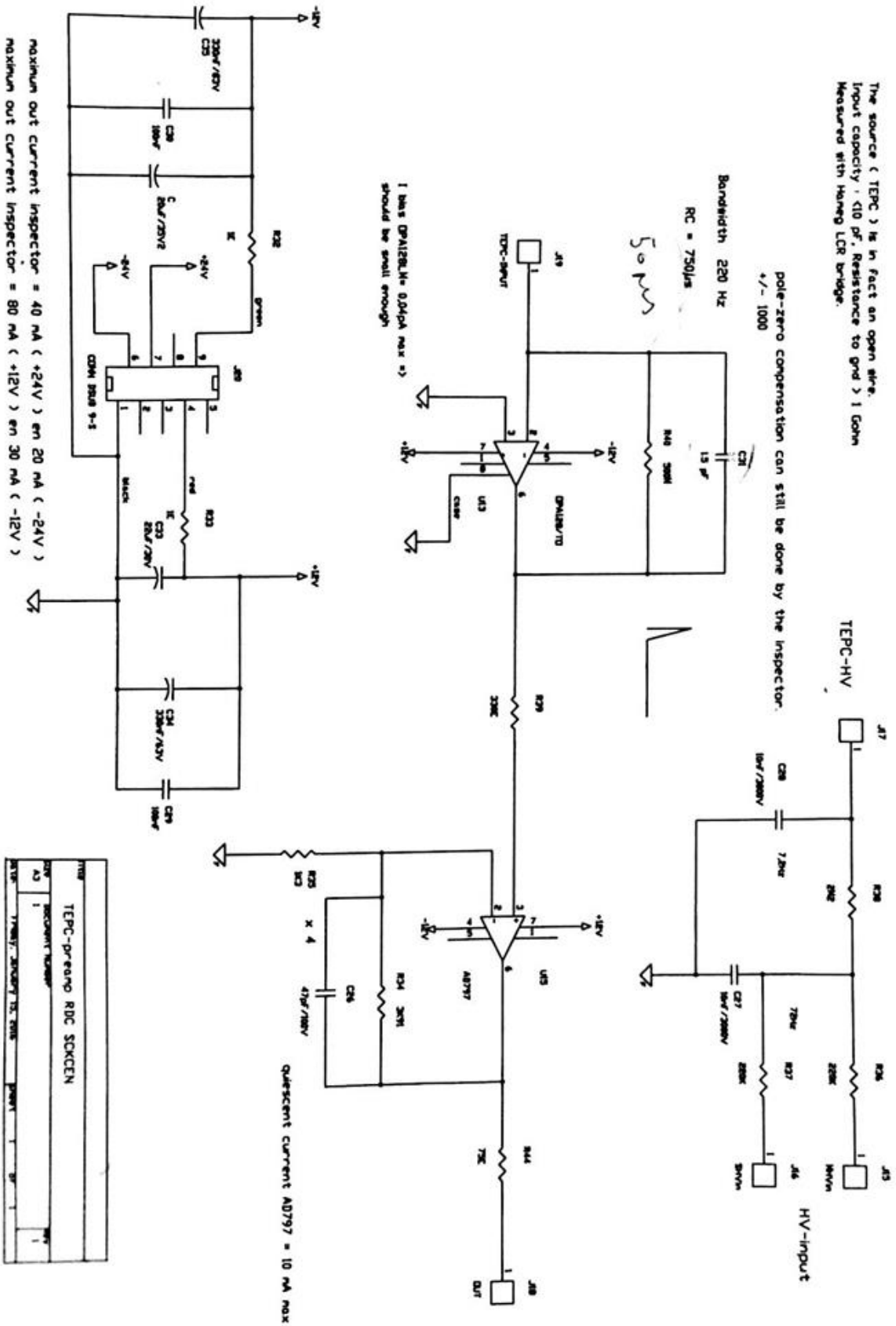

Figure A.3 – Scheme of the SCK preamplifier (Version 1).

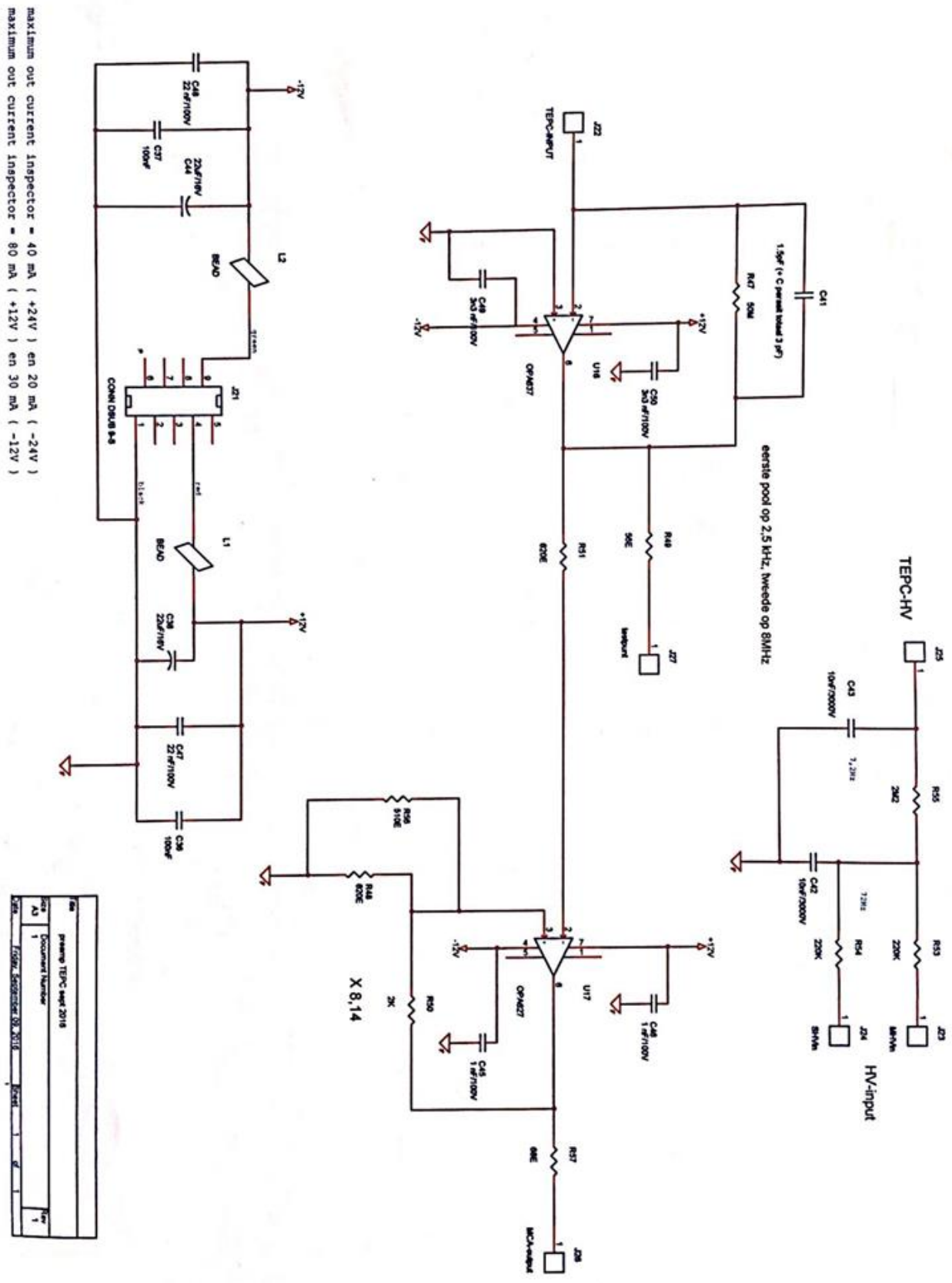

Figure A.4 - Scheme of the SCK preamplifier (Version 2).

Nomenclature

d	Cavity Diameter, [m]
ρ_g	Density of the Tissue Equivalent Gas, [kg/m^3]
V	Applied Voltage on the TEPC, [V]
Mg	Mass of the Gas in the Cavity, [g]
P	Required Tissue Equivalent Gas Pressure, [Pa]
T	Required Tissue Equivalent Gas Temperature, [K]
X_t	Path Length Across the Simulated Tissue, [µm]
X_g	Path Length Across the Gas Cavity, [cm]
y	Lineal Energy, [keV/µm]
ε	Imparted Energy, [keV]
$\bar{l}$	Mean Chord Length, [µm]
CF	Calibration Factor, [keV/µm/Channel Number]
LET	Linear Energy Transfer, [keV/µm]
D	Absorbed Dose rate, [µGy/h]
σD	Uncertainty on the Absorbed Dose Rate, [µGy/h]
Q	Quality Factor, [Sv/Gy]
σ_Q	Uncertainty on the Quality Factor, [Sv/Gy]
$\sigma_Q/Q(\%)$	Percentual Uncertainty on the Quality Factor
H	Dose Equivalent Rate, [µSv/h]
σ_H	Uncertainty on the Dose Equivalent Rate, [µSv/h]
$\overline{y_D}$	Dose Mean Lineal Energy, [keV/µm]
$\overline{y_F}$	Frequency Mean Lineal Energy, [keV/µm]
σ_{yD}	Uncertainty on the Dose Mean Lineal Energy, [keV/µm]
σ_{yF}	Uncertainty on the Frequency Mean Lineal Energy, [keV/µm]
$\sigma_{yD}/yD(\%)$	Percentual Uncertainty on the Dose Mean Lineal Energy
$\sigma_{yF}/yF\,(\%)$	Percentual Uncertainty on the Frequency Mean Lineal Energy

d(y)	Dose Probability Density
f(y)	Lineal Energy Frequency Distribution

Acronyms

ADC	*Analog to Digital Converter*
DPP	*Digital Pulse Processor*
MCA	*Multi Channels Analyzer*
TEPC	*Tissue Equivalent Proportional Counter*
SCK	*Studiecentrum voor kernenergie*
CEN	*Centre d'étude de l'énergie nucléaire*
P/Z	Pole/Zero

BIBLIOGRAPHY

[1] D. Moro, S. Chiriotti, V. Conte, P. Colautti1 and B. Grosswendt, “LINEAL ENERGY CALIBRATION OF A SPHERICAL TEPC”, (Mar 2016).

[2] V. Conte, D. Moro, B. Grosswendt, P. Colautti, “Lineal Energy Calibration Of Mini Tissue-Equivalent Gas-Proportional Counters (TEPC)”, (2012).

[3] H.H. Rossi M. Zaider, “Microdosimetry and its Applications”, (1996).

[4] K.M. Langen, P.J. Binns, A.J. Lennox, T.K. Kroc, P.M. DeLuca Jr., “Pileup correction of microdosimetric spectra”, (2002).

[5] S.N. Al-Bayati, “The Application of Experimental Microdosimetry to Mixed-Field Neutron-Gamma Dosimetry”, (2012).

[6] S. Chiriotti, “Microdosimetry of hadron therapy beams using mini Tissue-Equivalent Proportional Counters”, (Oct 2015).

[7] S. Chiriotti, D. Moro , V. Conte, B. Grosswendt, F. Vanhavere, S. Vynckier, “Indirect method to monitor the site size of sealed TEPCs”, (2016).

[8] J.F. Dicello, W. Gross, U. Kraljevic, “Radiation quality of californium-252”, in Physics in medicine and biology (1972).

[9] S. Gerdung, P. Pihet, J.E. Grindborg, H. Roos, U.J. Schrewe, and H. Schuhmacher, “Operation and Application of Tissue Equivalent Proportional Counters”, in Radiat Prot Dosimetry (1995)

[10] Glenn F. Knoll, “Radiation Detection and Measurement”, (Aug 2010).

[11] A.J. Waker, “Principals of Experimental Microdosimetry”, in Radiat Prot Dosimetry (1995).

[12] Aslam and A. J. Waker, “A study of neutron radiation quality with a tissue-equivalent proportional counter for a low-energy accelerator-based *in vivo* neutron activation facility”, in *Radiat Prot Dosimetry* (2011).

[13] G.M. Spirou, S.H. Byun and W.V. Prestwich, "Comparison of Three Pulse Processing Systems for Microdosimetry," in *IEEE Transactions on Nuclear Science* (Oct. 2008).

[14] A.J. Waker, K. Szornel, and J. Nunes, “TEPC Performance in the CANDU Workplace” in *Radiat Prot Dosimetry* (1997).

[15] M.S. Stark, A.J. Waker, and J.B. Hunt, “The Determination of Fluence to Dose Equivalent Conversion Factors for Americium-Beryllium and Californium Sources

from Microdosimetric Measurements” in *Radiat Prot Dosimetry* (1987).

[16] ICRU, Microdosimetry, Report 36, International Commission on Radiation Units and Measurements, (1983).

[17] CAEN , "WP2081 digital pulse processing in nuclear physics" (Aug 2011).

[18] CAEN, “Energy Resolution and Linearity of the MCA CAEN DT5780”, (Jan 2014).

[19] CAEN, “UM3182 MC^2Analyzer User Manual Software for digital Multi Channel Analyzer”, (Jan 2015).

[20] Canberra Industries, “Model 1300 InSpector 2000 Hardware Manual”, (2001).

[21] Canberra Industries, “ Model 2006 Proportional Counter Preamplifier”, (2007).

[22] Advanced Measurement Technology ORTEC®, “Model 142PC Preamplifier Operating and Service Manual”, (2002).

[23] Far West Technology Inc., “OPERATION MANUAL Model LET-SW5”, (Apr 2010).

[24] Https://www.sckcen.be/en/Research/Infrastructure/BR1